Norwegian University
of Life Sciences

Master's Thesis 2016 30 ECTS
Institutt for matematiske realfag og teknologi

A Mathematical Model of Biphasic Intracellular Calcium Dynamics in Hormone Producing Cells

Eirik Hovind
Miljøfysikk og fornybar energi

Acknowledgement

I wish to acknowledge the help provided by Geir Halnes, Kjetil Hodne, Gaute Einevoll and Finn-Arne Weltzien.

Special thanks to Geir Halnes for all the guidance throughout this semester,

and Kjetil Hodne for providing data and teaching biology
.

Eirik Hovind

Abstract

Synthesis and release of the two gonadotropins FSH and LH is dependent on increased levels of intracellular Ca^{2+}. In mammalian gonadotropes, different Ca^{2+} patterns have been observed, including oscillatory and mo-nophasic Ca^{2+} responses following GnRH stimulation. On the other hand, in teleost fish, monophasic and biphasic Ca^{2+} response has been observed. The biphasic response observed in the LH producing cells from medaka (*Oryzias latipes*), a teleost fish model, consists of an initial peak in intracellular Ca^{2+} level, due to release from endoplasmic reticulum. This is followed by a second plateau phase due to increased influx of Ca^{2+} from extracellular space, mediated by voltage activated Ca^{2+} channels (L-type). As a part of understanding Ca^{2+} signaling in gonadotropic cells, we employed a mathematical model describing the biphasic response observed in LH producing cells of the medaka. In order to explain this Ca^{2+} response, we used a model to describe intracellular Ca^{2+} dynamics together with a model of L-type channels. To the best of our/my knowledge, no mathematical model of intracellular Ca^{2+} dynamics in teleost gonadotrope cells exist. As a result, we employed a model of intracellular Ca^{2+} dynamics in mammalian gonadotropes. The mammalian model describes only the first part of the biphasic Ca^{2+} response mediated by the inositol triphosphate(IP3) activated Ca^{2+} release from endoplasmic reticulum. Secondly, we employed a Hodgkin Huxley type model of L-type channels on the plasma membrane, which produced an influx of Ca^{2+} into the cytosol. Together, we showed that these mechanisms formed the biphasic response.

Sammendrag

Syntese og frisetting av gonadotropinene FSH og LH er avhengig av økt nivå av intracellulært Ca^{2+}. I gonadotrope celler hos pattedyr har det blant annet blitt observert oscilerende og monofaskiske Ca^{2+} responser, mens i teleoster er det funnet bifasiske og monofasiske Ca^{2+} responser. Den bifasiske responsen observert i lh produserenede celler hos medaka (*Oryzias latipes*), en mye benyttet modellfisk, består blant annet av en økning av intrcellulært Ca^{2+} frigjort fra endoplasmatisk retikulum (ER). Denne Ca^{2+} toppen er etterfulgt av et nytt Ca^{2+} platå som følge av økt Ca^{2+} innfluks fra ekstracellulære rom/væsken gjennom spenningsaktiverte Ca^{2+} kanaler (L-type). For å forstå Ca^{2+} signalisering i gonaodotrope celler, brukte vi en matematisk modell for åforklare den bifasiske responsen observert i Lh produserende gondadotroper. For å gjennskape denne responsen måtte vi bruke en modell som både forklarer L-type kanaler og intracellulære mekanismer. Såvidt vi vet finnes det ingen matematiske modeller av Gnrh inusert Ca^{2+} respons i gonandotrope celler hos teleost. Derfor måtte vi bruke en allerede utviklet modell som beskriver Ca^{2+} responsen til gonadotrope celler hos pattedyr ved GnRH stimulering. Pattedyrmodellen forklarer kun den første delene av den bifasiske responsen der Ca^{2+} blir frigitt til cytosol gjennom inositol tripfosfat (IP3) aktiverte Ca^{2+} kanaler på ER membranen. Samtidig brukte vi en Hodgkin Huxley type modell av L-kanaler, som skapte en innstrømning av Ca^{2+} gjennom plasma membranen. Sammen skapte modellene den bifasiske responsen.

Contents

1 Introduction

Calcium ions play an fundamental part in virtually all aspects of intracellular signaling, including hormone regulation, synaptic plasticity, and gene regulation [2][8][18]. With changing environment, cells must react with changed signaling. In order to change, information of the change has to be stored. Calcium ions (Ca^{2+}) fills this role in the sense that the cytoplasmic Ca^{2+} concentration ($[Ca^{2+}]_i$) changes over time [2]. The $[Ca^{2+}]_i$ will influence intracellular mechanisms such as protein conformations and electrostatic fields[3]. Because of this, it is important for the cell to regulate $[Ca^{2+}]_i$. Intracellular concentration of free Ca^{2+} are as low as 100 nm, while extracellular Ca^{2+} are in the range of mM. In order to maintain this large plasma membrane Ca^{2+} gradient the cell must control the intracellular Ca^{2+} levels through buffers and plasma membrane pumps [3].

Among the variety of Ca^{2+} responses observed in cells we find both oscillatory and biphasic patterns [10] [18]. These alternations in $[Ca^{2+}]_i$ typical combines release of $[Ca^{2+}]$ into the cytoplasm from internal stores followed by increase influx of Ca^{2+} over the cell membrane. Both oscillatory and biphasic responses are found in a number of excitable endocrine (hormone producing) cells. In particular, we find a subset of endocrine cells situated in the pituitary that produce and release follicle-stimulating hormone (FSH) and luteinizing hormone (LH). These two hormones regulates gonadal development and is synthesized and released into the blood when stimulated with gonadotropin-releasing hormone (GnRH) from the hypothalamus [18]. Importantly, the $[Ca2+]_i$ determines the amount of FSH and LH produced and released. The signaling transduction in mammalian gonadotropes are well studied, however biological questions still remains unanswered. What differentiate cells that produce more FSH to those favouring production of LB is still unknown [18]. In mammalian gonadotropes FSH and LB are produced in the same cells, while in teleost cells either specialize in FSH or LB production and release [18]. Understanding the mechanisms that differentiates the GnRH signaling transduction in LH and FSH producing cells in teleost can lead to insights regarding differentiating factors of LH and FSH in the GnRH signaling transduction of mammalian gonadotropes.

As a part in understanding the GnRH signaling transduction, knowledge behind mechanisms controlling the $[Ca^{2+}]_i$ variations is highly important. In mammalian gonadotropic cells, it has been experimentally shown that the cell produces $[Ca^{2+}]_i$ oscillations with a frequency depending on stimulated GnRH concentration [10]. This, however, has not been observed in teleost gonadotropes. In the teleost fish medaka (*Oryzias latipes*) a monophasic or biphasic $[Ca^{2+}]_i$ response to GnRH has been observed, as shown in figure 1. Both the monophasic and biphasic responses to GnRH consists of an initial $[Ca^{2+}]_i$ increase, which is believed to mainly consists of Ca^{2+} released from inositol triphosphate (IP3) activated Ca^{2+} channels on the ER (endoplasmic reticulum) membrane. IP3 is part of the GnRH signaling transduction pathway. The biphasic response also consists of a second $[Ca^{2+}]_i$ plateau. When gonadotropic cells are stimulated with GnRH, potassium ion (K^+) channels on the plasma membrane may be inactivated causing the cell to depolarize and fire action potentials[18] [17]. Action potentials activates voltage activated Ca^{2+} channels (VACC) on the plasma membrane [18] which release Ca^{2+} into the cytosol from extracellular space.

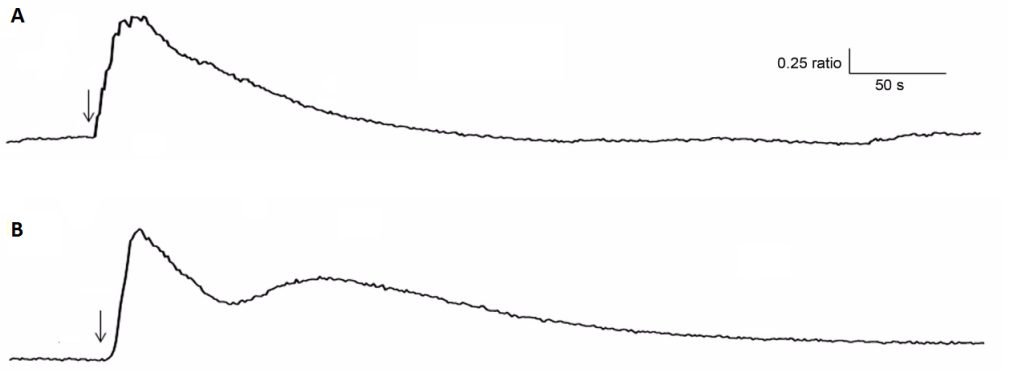

Figure 1: The original recordings of relative increase in $[Ca^{2+}]_i$ during GnRH stimulation. Figure A shows a monophasic response to GnRH while figure B shows a biphasic response. The black arrow is the onset of GnRH stimulation. [18]

There are many models of mammalian cells describing intracellular mechanisms, such as IP3 mediated Ca^{2+} release from ER [10][25][4]. The Ca^{2+} dynamics are dictated by the IP3 activated Ca^{2+} channels on the ER membrane, which are often explained by complex kinetic schemes [25][15]. Young and Keizer were the first to describe Ca^{2+} oscillations in mammalian cells with a model directly based on biophysical mechanisms, and contains as many as nine variables [9]. This model was simplified by Li *et al.* [9] by making various assumptions regarding the biophysical mechanisms. They developed a Hodgkin Huxley type formalism [9], and eventually reproduced experimental recordings of mammalian gonadotropic $[Ca^{2+}]_i$ oscillations using their simplified model [10]. As of April 2016, to the best of the author's knowledge, no mathematical models existed of the monophasic and biphasic Ca^{2+} responses experimentally observed in teleost gonadotropic cells. The objective of this thesis was, therefor, to develop such a model, and study the underlying mechanisms of $[Ca^{2+}]_i$ signaling in teleost gonadotropes through mathematical models. Our focus will be to reproduce the Stranabø experimental data, namely the biphasic response.

In order to reproduce the Ca^{2+} response, a mechanism which models the intracellular Ca^{2+} dynamics of cytosol and ER has to be included. The Li *et al.* 94 [10] model was chosen for this purpose, since it is relatively simple and one of the few models specializing on gonadotropes. We will refer to this module as LR (Li and Rinzel). The module will handle phenomena such as IP3 mediated Ca^{2+} release from ER, and various Ca^{2+} pump/exchanger activity on the plasma membrane and ER membrane. We refer to the article from which we obtained the model as the LR article. We will also construct our own module which governs the simulation of action potentials including VACC on the plasma membrane through Hodgkin Huxley type models. The VACC will release Ca^{2+} into the cytosol with each action potential. We will refer to this module as FD (fire dependent), as in dependence on firing of action potentials to release Ca^{2+} into the cytosol. Our hope is that this module in conjunction with the LR module will produce the second part of the biphasic response, as shown in figure 1.

In chapter 3 elemental biophysical theory for computational neuroscience is introduced. Chapter 4 describes the mathematical models used in the current work, and briefly describes how the model equations were solved. In chapter 5.1 we present the Ca^{2+} dynamics as predicted by the LR-module, while chapter 5.1.2 we present the Ca^{2+} influence predicted by the FD-module. In the final part of the result section, we combine the LR and FD models into the full model, and compare our simulation with the biphasic response observed in medaka (shown in figure 1). Lastly, in chapter 6 discuss our results, comment possible model limitations and suggest possible ways to improve the model in future work.

2 Abbreviations

ER: Ectoplasmatic reticulum
LR: Li and Rinzel (authors of Li *et al.* [10] article)
FD: Fire dependent
VDCC: Voltage dependent calcium channels
GHK: Goldman Hodgkin Katz
GnRH: Gonadotropin-releasing hormone
$[\boldsymbol{Ca^{2+}}]_{\boldsymbol{er}}$: The ER concentration of free Ca^{2+}
$[\boldsymbol{Ca^{2+}}]_{\boldsymbol{i}}$: The cytosol concentration of free Ca^{2+}
IP3: inositol triphosphate
SERCA: sarco/endoplasmic reticulum Ca^{2+}-ATPase

3 Computational background

Excitable cells such as gonadotropes produce signals by letting ion fluxes cross the plasma membrane. These fluxes changes both electrical potential energy and ion concentrations on the inside and outside of the plasma membrane.

3.1 The neural membrane

The cell membrane is mostly made out of the lipid bilayer, which by itself is not penetrable for ions. However, some proteins makes up ion channels, pumps and exchangers situated on the plasma membrane. These will at certain times let the ions pass. Cells carry several ion types, the most common being Na^+, K^+, chloride (Cl^-) and Ca^{2+}. The concentration of each ion usually varies very little from either side of the membrane.

Ion channels do not need energy to move ions, as drift and diffusion naturally creates a net flux of ions when the channels are open. The next sections will go through this in detail. However, ion channels are usually closed, and can only be activated by a certain voltage across membrane or by a molecule that binds to its receptor, which is situated next to the channel. It is important to note that ion channels are selective, meaning that specific ion channels favours flow of certain ion types. In the following sections we will go through how ion flow through these channels can be mathematically modeled.

Plasma membrane pumps and exchangers, on the other hand, forces ions across the plasma membrane, and require energy in order to operate. They often get their energy from the highly energetic molecule ATPase [12]. These pumps and exchangers also favour certain ion types. For example the Ca^{2+} ATPase pump on the plasma membrane and on the ER membrane make certain that the intracellular Ca^{2+} resting concentration is only about 0.01 - 0.10 µM, while the extracellular concentration can be as much as a few mM. As we will see $[Ca^{2+}]_i$ can increase to up to 1 µM, but the exchangers and pumps will always make sure these levels eventually decline to the resting level. Section 3.3 describes how these mechanism can be modeled, and what assumptions are made.

3.2 Ion fluxes across membrane channels

One often assumes that two physical phenomena create an ionic current across a membrane. These are diffusion and electrical drift. Diffusion is a random phenomenon due to collisions on a microscopic level, also known as Brownian motion [12]. However, on a macroscopic level one can statistically dictate how population of particles tend to move. This is described by the one dimensional diffusion equation:

$$J_{S,diff} = -D_S A \frac{d[S]}{dx} \tag{1}$$

Where $D_S(\mathrm{cm\,s^{-1}})$ is the diffusion coefficient, which describes how fast the population of particles $[S]$(M) diffuse [10]. $A(\mathrm{cm}^2)$ is the area of the surface perpendicular to $J_{S,diff}$. S is the ionic species, and J_S is the ion flux, which has units $(\mathrm{mol\,s^{-1}})$. Notice the molar current J_S moves in the direction of less concentration, so as time goes by all the particles will be evened out if not

affected by other physical phenomena. We will use equation 1 to describe the flux across a membrane, and we assume that the concentration gradient across the two other dimensions are zero. The other ion flux across the membrane is due to drift. Populations of ions will create electrical fields. These fields will accelerate the particles, but the particles will eventually collide with other molecules at increasing speeds which will force them to stop. This process is repeated, and on a macroscopic level one can observe a tendency of charged particles to move in an direction of decreasing electric potential. By linking the mobility of the particles [12] with the diffusion coefficient it is possible to obtain a mathematical expression describing the tendency of particles to move on a macroscopic level:

$$J_{S,drift} = -\frac{D_S F}{RT} z_S [S] A \frac{d\psi}{dx} \tag{2}$$

D_S is again the diffusion coefficient, F is Fardays constant, R is the gas constant, T temperature and z_S the valence of the ions. A is the area perpendicular to $J_{S,drift}$. $-\frac{d\psi}{dx}$ tells us that the particles move in the direction of less electrical potential energy where ψ is the local potential. We now summarize the physical effects on ionic flux of species S across the plasma membrane [16]:

$$J_S = J_{S,dirft} + J_{S,diff} = -D_S A \left(\frac{d[S]}{dx} + \frac{z_S F}{RT} [S] \frac{d\psi}{dx} \right) \tag{3}$$

From this equation one can quickly deduce the relationship between the potential across the membrane and $[S]$ on either side of the membrane when the net flux is zero. The net flux is zero when

$$-\frac{d[S]}{dx} = \frac{z_S F}{RT} [S] \frac{dV\psi}{dx}$$

We can integrate this expression in a straight line across the membrane, where we set $[S]_o$ as the concentration just outside the membrane in extracellular space, and $[S]_i$ is the concentration on the inside. $\psi = 0$ on the outside of the membrane by convention, and $\psi = E_S$ on the inside. We integrate across the membrane from the inside to the outside:

$$\int_{E_S}^{0} -d\psi = \int_{[S]_i}^{[S]_o} \frac{RT}{z_S F [S]} d[S]$$

And we obtain the Nernst equation:

$$E_S = \frac{TR}{z_S F} \frac{[S]_o}{[S]_i} \tag{4}$$

This equation tells us that when the voltage across the membrane $V = E_S$ there is no flux of ion S across the membrane, but reversely when $V \neq E_S$ there will be.

3.2.1 The Goldman Hodgkin Katz current equation

The Goldman Hodgkin Katz current equation describes the ion current across a membrane, depending on voltage and ion concentration on either side. Figure

2 describes our situation with initial conditions. We use equation 3, and convert to current with $i_S = Fz_S J_S / A$. F is Faraday's constant and z is again the valency of ion S. So that

$$i_S = -z_S F D_S \left(\frac{d[S]}{dx} + \frac{z_S F}{RT}[S]\frac{d\psi}{dx} \right) \tag{5}$$

which we multiply with integrating factor [7]:

$$i_S = -z_S F D_S \frac{e^{z_S F\psi}}{e^{z_S F\psi}} \left(\frac{d[S]}{dx} + \frac{z_S F}{RT}[S]\frac{d\psi}{dx} \right) \tag{6}$$

And by using the product rule of derivatives one obtains:

$$i_S = -\frac{z_S F D_S}{e^{Z_S F\psi/RT}} \frac{d}{dx}([S]e^{Z_S F\psi/RT}) \tag{7}$$

Then we rearrange and integrate as pictured in figure 2, from just inside the

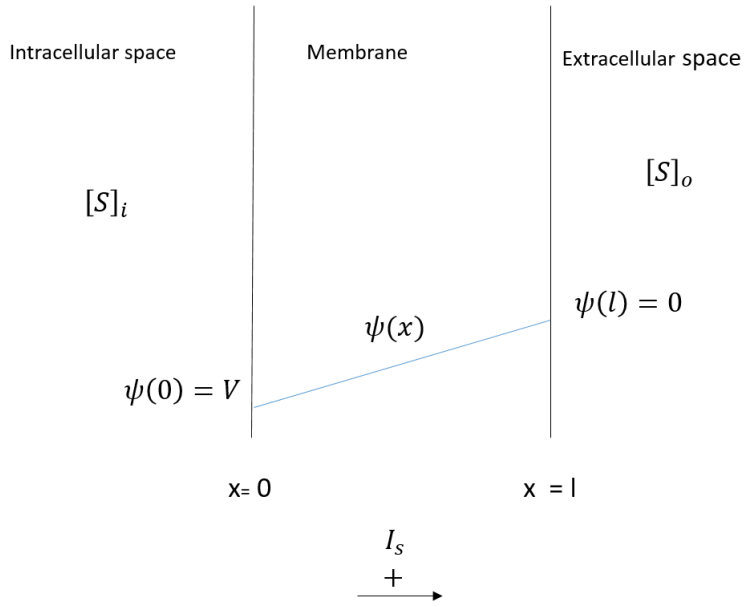

Figure 2: Figure showing the boundary condition of our membrane, and how the local voltage ψ is assumed varying linearly with respect to x inside the membrane. i_s is constant for all x. [7]

plasma membrane to the other edge:

$$\int_0^l i_S \frac{e^{Z_S F\psi/RT}}{z_S F D_S} dx = -\int_0^l \frac{d}{dx}([S]e^{Z_S F\psi/RT})dx \tag{8}$$

Now, assuming that i_S is the same for all x. We use the partition coefficient $\beta*$ to describe the relationship between the concentration just inside the membrane, and outside the membrane so that $[S](0) = [S]_i \beta_S^*$ and $[S](l) = [S]_o \beta_S^*$ [7]. We use ψ as from figure 2: $\psi = (V - xV/l)$, and assume D_S^* is constant.

For simplicity we use $v_s = Z_S FV/RT$.

$$i_S \int_0^l \frac{e^{(V-xV/l)Z_S F/RT}}{D_S} dx = -z_S F(\beta_S^*[S]_o e^{Z_S F0/RT} - \beta_S^*[S]_i e^{Z_S FV/RT}) \quad (9)$$

$$i_S \frac{e^{VZ_S F/RT}}{D_S} \int_0^l e^{-xVZ_S F/lRT} dx = -z_S F\beta_S^*([S]_o - [S]_i e^{v_s}) \quad (10)$$

$$-i_S \frac{e^{v_s}}{D_S} \frac{lRT}{VZ_S F} \left[e^{-lVZ_S F/lRT} - e^{-0VZ_S F/lRT}\right] = -z_S F\beta_S^*([S]_o - [S]_i e^{v_s}) \quad (11)$$

And in the end rearranging and simplifying:

$$i_S e^{v_s} = \frac{z_S^2 F^2 V \beta_S^* D_S}{lRT} \frac{([S]_o - [S]_i e^{v_s})}{(e^{-v_s} - 1)} \quad (12)$$

In the end we obtain the Goldman Hodgkin Katz current equation by setting $P_S = \beta_S^* D_S^*/l$ which is the permeability [7].

$$i_S = \frac{P_S z_S^2 F^2 V}{RT} \frac{[S]_i - [S]_o e^{-Z_S FV/RT}}{1 - e^{-Z_S FV/RT}} \quad (13)$$

3.2.2 Simplifications

Ion currents across open ion channels can be expressed with equation 13, but can usually be simplified in the case of Na^+ and K^+ ion channels. When these ion channels are open, the concentration of Na^+ and K^+ on either side of the membrane does not change considerably [16]. This means that the equilibrium potential E_S expressed by equation 4 is constant. As it turns out, in the case of Na^+ and K^+ the current I from equation 13 has the property that $i \propto (V - E_S)$ to a certain degree [16], where V is the voltage across the membrane and E_S the equilibrium potential of ion type S. Another way of formulating this is to characterize the current i_S as quasi-ohmic, meaning that the current can be described as a battery in series with a resistor. The description of the current then becomes:

$$i_S = \bar{g}(V - E_S) \quad (14)$$

E_s is then the voltage of the battery and $\bar{g}$ the inverse of the resistance of the resistor, also known as conductance. By taking into account the fraction of open ion channels, one get the current:

$$i_S = a\bar{g}(V - E_S)$$

where a is the fraction of open channels. $a\bar{g}$ is now the inverse of a varying resistance. Additionally one keeps track of the total amount of ions in the cell by modeling the membrane as a capacitor, so that the capacitor determines the voltage across the membrane. Figure 3 , shows the different currents in parallel with each other and the capacitor. The leak current however consist of various currents not explained by sodium or K^+ ion channels [16]. When dealing with Ca^{2+} one cannot make this simplification by express the current as equation 14 instead of equation 13. This is because the intracellular Ca^{2+} concentration changes considerably when the Ca^{2+} ion channels are activated. In other words the Nernst potential is not constant, neither does the current expressed by equation 13 for Ca^{2+} possess quasi ohmic properties.

3.2.3 The action potential

In 1952 Hodgkin and Huxley managed to mathematically model the action potential of the squid giant axon [16]. Their work defined the way in which one models ion channels to this day. They experimentally recorded current voltage relations of ion channels with the voltage clamp technique. To model their data, they made the assumption that the ion channels belonging to ion type S could be either in an open or closed state. Each ion channel could also have several ion gates in a row. For example, if the opening probability of a channel is n and the ion type has x amount of gates per channel the amount of open channels becomes n^x where each gate has the same properties [16]. The fraction of open gates were then dictated by a chemical reaction:

$$C \underset{\beta_n}{\overset{\alpha_n}{\rightleftharpoons}} O$$

the fraction of open channels O are then n, while the ones closed are naturally $1 - n$. Here $\beta_n(V)$ is the rate at which open gates becomes closed and $\alpha_n(V)$ the rate closed gates becomes open. So that:

$$\frac{dn}{dt} = \alpha_n(V)(1 - n) - \beta_n(V)n \tag{15}$$

This is can be simply integrated since α_n and β_n is time independent:

$$n = \frac{\alpha_n}{\alpha_n + \beta_n} + \left(n_0 - \frac{\alpha_n}{\alpha_n + \beta_n} \right) e^{-(\alpha_n + \beta_n)t}$$

This expression can be compared with the experimentally observed ion channel openings when isolated K^+ currents experiencing a voltage jump. n_0 is just the initial channel openings. One can rewrite this by setting $n_\infty = \frac{\alpha_n}{\alpha_n + \beta_n}$ and $\tau_n = \frac{1}{\alpha_n + \beta_n}$:

$$n = n_\infty + (n_0 - n_\infty)e^{-t/\tau_n}$$

Determining n_∞ and τ_n is just the same as setting values for α_n and β_n. This means that fitting n_∞ and τ_n to experimental data has a sort of physical basis. It can be shown that equation 15 is the same as:

$$\frac{dn}{dt} = \frac{n_\infty - n}{\tau_n} \tag{16}$$

Now for example if one chose four gating particles as Hodgkin and Huxley did in the case of K^+ [16], and experimentally record the equilibrium conductance $g\bar{_{K_\infty}}$ for K^+ at voltage V_1 n_∞ is then:

$$n_\infty(V_1) = \left(\frac{\bar{g}_{K_\infty}(V_1)}{\bar{g}_K} \right)^{1/4}$$

Now $n_\infty(V)$ one can fitted to suit all relevant V. $\tau_n(V)$, on the other hand, has to be chosen as to fit the time course of the signal [16]. However, in the case Na^+ current only one gating particle type is not sufficient in describing how the current reacts to varying voltage. When the Na^+ experiences an voltage

change, the ion channels will activate and produce a current, but after a while this current will decline. In order to model this, it is possible to use a combination of inactivation variables and closing variables. Three particles will activate with increasing voltage and so increase the current, and a delayed particle will eventually close and stop the current. The two types of particles has different kinetics, so that the time course of the Na^+ current can be fitted with four parameters instead of two.

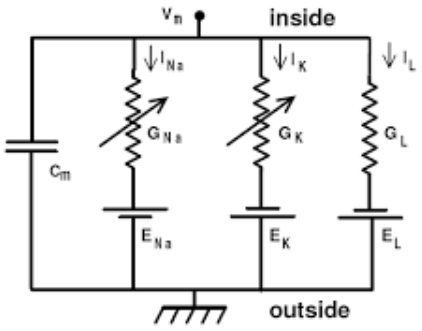

Figure 3: The equivalent circuit of membrane voltage mechanisms [13].

Together, the Na^+ and K^+ currents form the action potential. Increasing voltage activates the Na^+ current, which increases the voltage over the membrane by depolarize the cell. While the voltage across the membrane increases, the K^+ kinetics starts to activate. As K^+ current forces the current in the opposite direction and Na^+ current is inactivated by the inactivating variable, the voltage eventually decline. At low voltage both currents are inactivated. The leak current forces the voltage back to the resting potential.

3.2.4 Types of Hodgkin Huxley models

Generally, models inspired by Hodgkin and Huxley's work can be divided into two groups depending on their f - I characteristics. F-I is an abbreviation for firing - input-current, meaning that a certain constant input-current gives a certain action potential firing frequency (Hz). Models which we call type-2 has a discontinuous F-I relation, which means that they are unable to obtain certain firing frequencies no matter what the constant input current is. Type-1 on the other hand has a one-to-one correspondence between frequency and input current, so any frequency can be obtained when the input current is tuned correctly [16].

3.3 Pumps and exchangers

Ion Pumps and exchangers can often be modeled as a chemical reaction depending on the ion concentration $[S]$ from the ion store it pumps from:

$$[E] + n[S] \underset{k_1^-}{\overset{k_1^+}{\rightleftharpoons}} [EnS] \xrightarrow{k^c} [E] + n[P] \tag{17}$$

Which is referred as an enzymatic reaction [16], where $[E]$ is the enzyme concentration (or pump concentration) n number of ions required in the reaction, and P the product (ions on the other side of membrane). $[EnS]$ is the state at which the ions are connected with the pump. The rate r_1 at which $[EnS]$ is produced from $[E]$ and $[nS]$ is proportional to the density of the enzymes(pumps) times the density of each ion that has to hit the pump simultaneously [12][16]:

$$r_1^+ = k_1^+[E][S]^n$$

Which means that in the case of $n = 2$, the pump (or exchanger) needs two ions at once in order to pump them through. and also we have that

$$r_1^- = k_1^-[EnS]$$

Naturally since $[EnS]$ is connected. We also have that $[EnS]$ can be released to the other side [16]:

$$r^c = k^c[EnS]$$

. Now we assume that that the reactions are always in equilibrium [16], so that

$$r_1^+ = r_1^- + r^c$$

and inserting for each:

$$k_1^+[E]_\infty[S]_\infty^n = k_1^-[EnS]_\infty + k^c[EnS]_\infty$$

with the equilibrium assumption leads to:

$$\frac{[E][S]^n}{[EnS]} = (k_1^- + k^c)/k_1^+ = K_m$$

And by setting $[E] = [E_{tot}] - [EnS]$ where $[E_{tot}]$ are total ion channels[16]:

$$\frac{([E_{tot}] - [EnS])[S]^n}{[EnS]} = K_m$$

$$[E_{tot}][S]^n - [EnS][S]^n = K_m[EnS]$$

$$[EnS]K_m + [EnS][S]^n = [E_{tot}][S]^n$$

which leads to

$$[EnS] = \frac{[E_{tot}][S]^n}{K_m + [S]^n}$$

The change of the product P (ions pumped out of membrane) [16]:

$$\frac{d[nP]}{dt} = k^c[EnS]$$

which is:

$$\frac{d[nP]}{dt} = k^c\frac{[E_{tot}][S]^n}{K_m + [S]^n}$$

This means that one can fit pump or exchanger rates to the equation:

$$J = V_{max}\frac{[S]^n}{K_m + [S]^n}$$

Where V_{max} is the maximum velocity of a concentration [16], K_m the apparent dissociation constant[12]. J is the flux out of the cell, which for example can have units $\mathrm{mol\,s^{-1}}$.

3.4 IP3-induced Ca^{2+} release

IP3 is part of GnRH signaling transduction and activates Ca^{2+} channels on the ER membrane. The kinetics of these channels are in reality very complicated, and difficult to model. Young and Kaizer modeled the IP3 activated Ca^{2+} channels as consisting of three independent gating particles [10]. Each particle had three activation/inactivation sites, one for activation by IP3, a second for activation by Ca^{2+} and a third for inactivation by Ca^{2+}. They formulated this into an eight state kinetic scheme, where populations of particles could transition between these states [5]. In 1994 Li et al. simplified their work, and formulated a Hodgkin Huxley like formalism much like the Na^{+} current:

$$J_{IP3} = a_\infty b_\infty d_\infty h([Ca^{2+}]_i - [Ca^{2+}]_{er})$$

So that the release from ER consists of four gating variables, a_∞ is activation with increasing $[Ca^{2+}]_i$, b_∞ is activation with IP3, d_∞ is activation with low $[Ca^{2+}]_{er}$ while h represents inactivation with high $[Ca^{2+}]_i$.

4 Methods

In this chapter, a mathematical model of Ca^{2+} dynamics in gonadotropic cells responding to external hormone stimulus is presented. The model include voltage over the plasma membrane and the Ca^{2+} concentrations in the cytosol and ER. Our model has no spatial dependencies, other than the obvious physical traits of a cell: The cytosol encloses the cell, so that Ca^{2+} fluxes through the plasma membrane only changes the ion concentration in the cytosol. The extracellular space is treated as having constant Ca^{2+} concentration and voltage.

4.1 Model overview

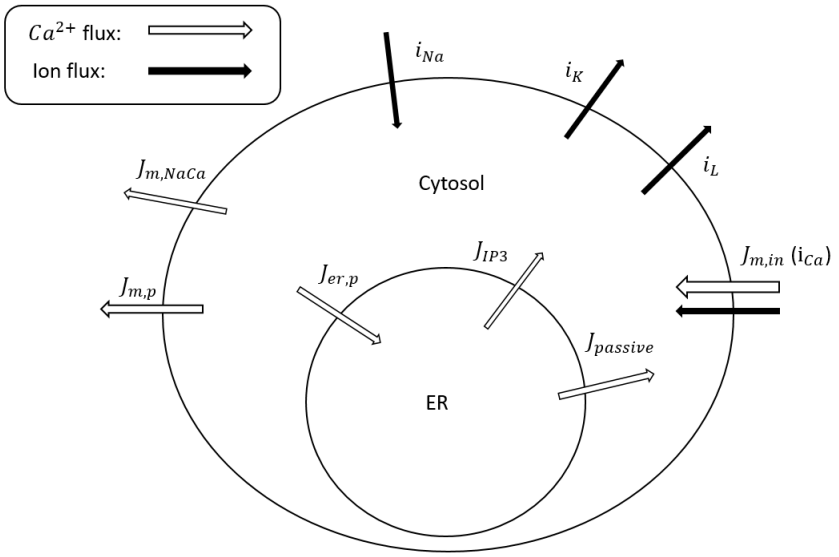

Figure 4: Figure indicating various ion fluxes through the plasma membrane, or the ER membrane. White arrows indicates Ca^{2+} ion fluxes which are part of the LR module. Black arrows indicate ion fluxes that changes the plasma membrane potential, which we refer to as the FD module. The Cytosol and ER functions as independent Ca^{2+} pools. $J_{m,in}$ is the only connection between the modules.

Figure 4.1 summarizes the model. It contained two Ca^{2+} compartments, i.e. the ER and cytosol, and fluxes of Ca^{2+} ions between these compartments. In addition, it included Ca^{2+} fluxes through the plasma membrane. These Ca^{2+} fluxes are depicted as white arrows in figure 4. The model that described the Ca^{2+} pools and the Ca^{2+} fluxes is what we referred to as the LR module, but in some cases except $J_{m,in}$. Section 4.3 describes the fluxes in detail. Black arrows, on the other hand, indicates ion fluxes that changed the plasma membrane voltage to a significant degree. Together these defined the FD module. The ion fluxes that altered the voltage were referred to as currents. i_{Na} was the current through the voltage activated Na^+ channels, i_K the current through the voltage activated K^+ channels, i_{Ca} was the current through the voltage activated Ca^{2+} channels and i_L was various other currents that also changes the potential. In section 4.2 we go through how these currents were mathematically modeled.

Equation 18 summarize the model of the voltage across the membrane:

$$C_m \frac{dV}{dt} = -i_L - i_{Na} - i_K - i_{Ca} - i_{input} \tag{18}$$

Where each current had units $\mu A\,cm^{-2}$. Electrical currents over the plasma membrane from exchangers and pumps were not included. This is because their current are small compared to ion channel currents during the action potential, which we will see in section 5.2.3. The equations governing the Ca^{2+} concentration in ER and the cytosol were as follows:

$$\frac{V_i}{f_i} \frac{d[Ca^{2+}]_i}{dt} = J_{IP3} + J_{passive} - J_{er,p} + J_{m,in} - J_{m,NaCa} - J_{m,p} \tag{19}$$

$$\frac{V_{er}}{f_{er}} \frac{d[Ca^{2+}]_{er}}{dt} = -J_{IP3} - J_{passive} + J_{er,p} \tag{20}$$

Here$[Ca^{2+}]_{er}$ is the free Ca^{2+} concentration in ER and $[Ca^{2+}]_i$ is the free Ca^{2+} concentration in the cytosol. Free concentration means concentration of ions able to move over the plasma membrane and ER membrane. Each flux had units $\mu mol\,s^{-1}$. V_i was the volume of the cytosol, V_{er} was the volume of the ER, f_i was the fraction of free Ca^{2+} in cytosol, and f_{er} was the fraction of free Ca^{2+} in ER. This means that $[Ca^{2+}]_{tot,i} f_i = [Ca^{2+}]_i$ where $[Ca^{2+}]_{tot,i}$ was the total Ca^{2+} in the cytosol including Ca^{2+} bound in various ways, and same with f_{er}. When we later refer to Ca^{2+} concentrations in cytosol and ER we refer to the concentration of free Ca^{2+} [10]. $J_{er,p}$ was the SERCA pump, which pumps Ca^{2+} from the cytosol into the ER. J_{IP3} was the IP3 activated Ca^{2+} channels which released Ca^{2+} from the ER into the cytosol, while $J_{passive}$ was various other Ca^{2+} fluxes from ER to cytosol not directly explained by our model. On the outer membrane we had $J_{m,NaCa}$, the Na^+/Ca^{2+} exchanger, and $J_{m,p}$, the Ca^{2+} ATPase pump. Both the pump and the exchanger moves Ca^{2+} from the cytosol into extracellular space. We go through each Ca^{2+} flux in detail in chapter 4.3. Equation 19 and equation 20 summarize the Ca^{2+} model.

As explained in figure 4, the i_{Ca} current consisted of Ca^{2+} ions and so also changed $[Ca^{2+}]_i$. This Ca^{2+} current was the only component which connected the equations governing the Ca^{2+} dynamics, equation 19 and 20, and the equation governing the voltage dynamics, namely equation 18. i_{Ca} was indicated through the $J_{m,in}$ component in equation 19. We converted i_{Ca} into $J_{m,in}$ by:

$$J_{m,in} = \frac{A}{z_{Ca} F} i_{Ca}$$

$A(cm^2)$ was the area of the plasma membrane, F was Faraday's constant $(mol\,C^{-1})$ and z (unitless) was the valency of the ion, which was 2 in our case. Notice that in some cases $J_{m,in}$ was modeled as a constant influx, since this freed us from modeling the membrane dynamics, in which case only equation 19 and 20 had to be solved in order to determine $[Ca^{2+}]_i$ and $[Ca^{2+}]_{er}$. Section 4.5.3 explains how the equations were rewritten in order to solve them numerically, and the software used. In the appendix we summarize all the equations which were directly solved through our software, and lists all relevant parameters in order to reproduce our results.

4.2 The FD module

In the following chapter we will define each current in equation 18, which together defines the FD module. All relevant parameters are listed in the appendix, table 1.

4.2.1 Na^+ and K^+ channels

In order to simulate action potentials we included a Hodgkin Huxley-type model of Na^+ and K^+ channels on the plasma membrane. The original Hodgkin Huxley model, described on p. 61 in Sterratt [16], is a type 2 model (see section 3.2.4 for description), and could not reproduce the firing pattern observed in our cell. We therefore chose to adapt a type 1 model of K^+ and Na^+ channels. We chose the model as originally described by Halnes *et al. 2011* [6]. With this model type, we managed to obtain satisfying firing frequency, as we will see later in in section 5.2.1. The Na^+ channel as appearing in equation 18 was expressed as follows:

$$i_{Na} = \bar{g}_{Na} m^3 h (V - E_{Na}) \tag{21}$$

Here, E_{Na} was the resting potential of the Na^+ channels, V was the voltage over the membrane, and m and h were the activation and inactivation variables respectively. $\bar{g}_{Na}$ was the conductance of the Na^+ channels. The conductance of the Na^+ and K^+ channels were tuned as to get a reasonable action potential shape. The final conductances are listed in table 1 in the appendix. The activation gating variable m, was described as follows:

$$dm/dt = (m_\infty - m)/\tau_m$$

Where

$$m_\infty = a/(a+b) \tag{22}$$

τ_m was described as follows:

$$\tau_m = \frac{1}{a+b} \cdot 3.0^{-(T-36)/10} \tag{23}$$

where T was in Celsius. The factor a and b for the Na^+ gating variable were:

$$a = 0.32 \cdot F(-V - 50, 4)$$

$$b = 0.28 \cdot F(V + 23, 5)$$

the function F was:

$$F(x,y) = \begin{cases} \frac{x}{e^{x/y}-1} & \text{if } |(x/y)| \geq 10^{-6} \\ y(1 - \frac{x}{y2}) & \text{if } |(x/y)| < 10^{-6} \end{cases} \tag{24}$$

While the inactivation gating variable h was described as follows:

$$dh/dt = (h_\infty - h)/\tau_h$$

h_∞ was:

$$h_\infty = a/(a+b) \tag{25}$$

while

$$\tau_h = \frac{1}{a+b} \cdot 3.0^{-(T-36)/10} \tag{26}$$

a and b were now

$$a = 0.128 \cdot e^{(-46-V)/18}$$

$$b = \frac{4}{1+e^{(-23-V)/5}}$$

The K^+ channel functioned as an delayed rectifier for the voltage across the membrane (see equation 18), as in the original Hodgkin Huxley model [16]. The equation governing the K^+ current was:

$$i_K = \bar{g}_K n^4 (V - E_K) \tag{27}$$

Which had the same form as equation 21 except it had no closing variable. E_K was the equilibrium potential, $\bar{g}_K$ was the maximum K^+ conductance, and n the gating opening probability. n was described as follows:

$$dn/dt = (n_\infty - n)/\tau_n$$

and as with the opening/closing variables for the Na^+ channel:

$$\tau_n = \frac{1}{a+b} \cdot 3.0^{-(T-36)/10} \tag{28}$$

$$n_\infty = a/(a+b) \tag{29}$$

Now a and b were expressed as follows:

$$a = 0.032 \cdot F(-48 - V, 5)$$

$$b = 0.5 \cdot e^{(-53-V)/40}$$

where $F(x, y)$ was given by equation 24.

4.2.2 Ca^{2+}-channel

As mentioned in section 4.1, for the Ca^{2+} flux through the plasma membrane we considered two different cases in our simulations. In some simulations, we used a simple constant Ca^{2+}-influx, the same as the one used in the original LR article. In other simulations, we modeled the influx current as depending on a Hodgkin Huxley type model of L-type channels. These channels open with increasing membrane voltage, and let Ca^{2+} pass through the membrane. The voltage gated L-type channel was modeled by the Goldman Hodgkin Katz current equation and a opening mechanism:

$$i_{Ca} = P_{Ca} m^2 \frac{z_{Ca}^2 F^2 V_m}{RT} \frac{[Ca^{2+}]_i - [Ca^{2+}]_o e^{-z_{Ca} FV/RT}}{1 - e^{-z_{Ca} FV/RT}} 10^{-3} \tag{30}$$

which is given a detailed explanation of in section 3. The gating mechanism and the final rewritten form were adapted from Halnes *et al.* [6]. Here, P_{Ca} was the maximum permeability (in units of dam s^{-1}), and $z_{Ca} = 2$ was the valence of the ion. F was Faraday's constant, R was the gas constant and T was the

temperature in kelvin. i_{Ca} had units $\mu A\,cm^{-2}$. The concentrations has units mM. The opening variable m of the channels was described as follows:

$$a = \frac{1.6}{1 + e^{-0.072 \cdot (V-12)}}$$

$$b = 0.02 \cdot \frac{V - 8.31}{e^{(V-8.31)/5.36} - 1}$$

$$\tau_m = \frac{1.0}{a+b} \cdot 3^{-0.1 \cdot (T-294.15)} \tag{31}$$

$$m_\infty = a/(a+b) \tag{32}$$

finally we have:

$$dm/dt = (m_\infty - m)/\tau_m$$

which can solved numerically. Figure 5 shows channel opening compared with voltage, while figure 6 shows the relaxation time constant dependency on voltage. T was the temperature in kelvin, we chose $T = 310.14$ K as in Halnes *et al.* [6]. Note that we used two different temperature values, the one listed in table 1 in the appendix was the temperature which goes directly into equation 30.

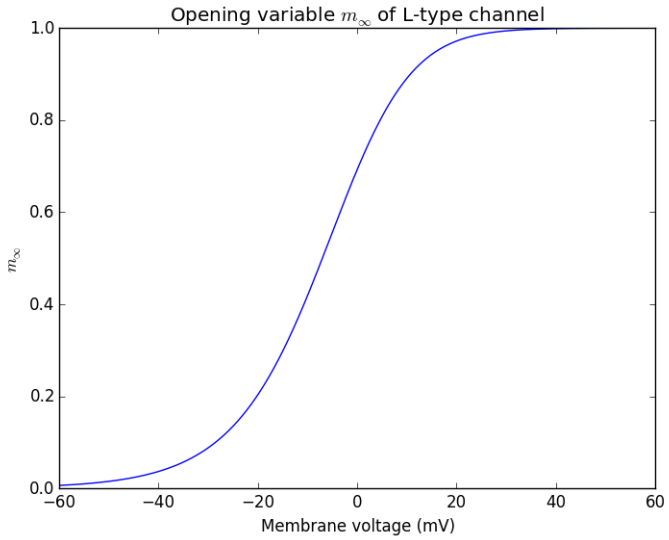

Figure 5: opening variable m_∞ of L-type channel.

4.2.3 Passive current through plasma membrane

As the passive current we chose:

$$i_L = \bar{g}_L(V - E_L) \tag{33}$$

The passive current is always open to flow through the membrane, in other words it does not have a activating gating variable. $\bar{g}_L$ was the conductance, and E_L the equilibrium potential. Both values were listed in table 1. V(mV) was as always the voltage across the membrane.

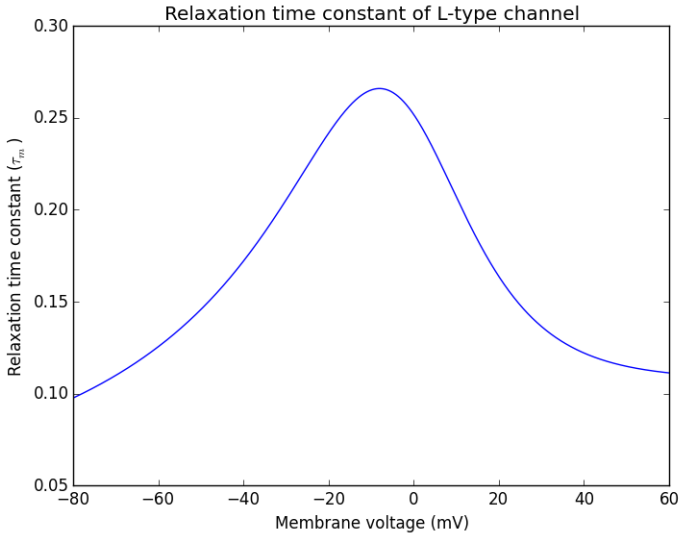

Figure 6: Relaxation time constant of L-type channel.

4.3 The LR module: Fluxes determining the Ca dynamics in cytosol and ER

We will now present all the components of the LR module as originally developed by Li *et al.* [10]. In the LR model, Ca^{2+} in the cytosol is determined by a balance of Ca^{2+} fluxes in the outer membrane, but also fluxes over the ER membrane. As pointed out in Li *et al.* [10] changing the leak permeability of the ER membrane, or the Ca^{2+} pump rate over the ER alters the current balance, and causes oscillation in the cytosol concentration. As mentioned in the beginning of the chapter, the equations governing the Ca^{2+} in cytosol and ER were:

$$\frac{V_i}{f_i}\frac{d[Ca^{2+}]_i}{dt} = J_{IP3} + J_{passive} - J_{er,p} + J_{m,in} - J_{m,NaCa} - J_{m,p}$$

$$\frac{V_{er}}{f_{er}}\frac{d[Ca^{2+}]_{er}}{dt} = -J_{IP3} - J_{passive} + J_{er,p}$$

We present each Ca^{2+} flux in detail below, while all relevant parameters for the Ca^{2+} dynamics can be found in table 2 in the appendix. Unless otherwise specified, the equations and parameters were taken from the original LR model [10].

4.3.1 $J_{passive}$

The expression for $J_{passive}$ was:

$$J_{passive} = P_{leak}([Ca^{2+}]_{er} - [Ca^{2+}]_i)$$

Where P_{leak} was constant. In a sense P_{leak} was the passive channel conductance, while $([Ca^{2+}]_{er} - [Ca^{2+}]_i)$ was the driving force as in a Hodgkin Huxley type model.

4.3.2 J_{IP3}

The $IP3$ activated Ca^{2+} flux was modelled as follows:

$$J_{IP3} = P_{ip3r} O([Ca^{2+}]_{er} - [Ca^{2+}]_i)$$

P_{ip3r} was the maximum conductance of the channels, modeled as a constant. The factor O consisted of four parameters:

$$O = a_\infty b_\infty d_\infty h$$

Which we give a quick explanation of in section 3.4. The opening probabilities a_∞, b_∞ and d_∞ had no time delay and were instantly activated or deactivated. The channel opening probability h on the other hand was dependent on time, and changed on a timescale of 20 seconds. a_∞, b_∞ and d_∞ were modeled after the Sigmoid function which was given by:

$$\Gamma(x, y, z) = 1/(1 + e^{(x-y)/z}) \tag{34}$$

So that:

$$a_\infty = \Gamma(0.4, [Ca^{2+}]_i, k_a) \tag{35}$$

Meanwhile b_∞ was expressed as:

$$b_\infty = \Gamma(0.45, IP3, 0.25) \tag{36}$$

the d_∞ was modeled as:

$$d_\infty = 0.5[1 + \Gamma([Ca^{2+}]_{er}, 2, 0.5)] \tag{37}$$

The opening probability of h was modeled by an ordinary differential equation:

$$dh/dt = (h_\infty - h)/\tau_h \tag{38}$$

Here h_∞ was also modeled by the Sigmoid function:

$$h_\infty = \Gamma([Ca^{2+}]_i, 0.35, k_h) \tag{39}$$

and the time constant τ_h was modeled as:

$$\tau_h = 1.5/(b_\infty d_\infty cosh[([Ca^{2+}]_i - 0.35)/0.18]) \tag{40}$$

Steepness parameters k_a, k_h, a_∞ and h_∞ depended on $IP3$. They had the form [10]:

$$k_a = \left(0.16 \frac{10}{10 + [Ca^{2+}]_{er}}\right) \left\{1 + \left(\frac{IP3}{0.2 + IP3}\right) \left(\frac{0.15^2}{0.15^2 + (IP3 - 0.25)^2}\right)\right\}$$

While

$$k_h = \left(0.46 \left[0.08 + \frac{[Ca^{2+}]_{er}(0.1^2 + IP3^2)}{[Ca^{2+}]_{er}(1 + IP3^2) + 8}\right]\right)$$

Where we slightly corrected the k_a term from the original article, see results for more details. The corrected form was also the one they used in their simulations. The dynamical parameters $[Ca^{2+}]_i$,$[Ca^{2+}]_{er}$ and $IP3$ that went into the equations k_a and k_h were in µM.

4.3.3 $J_{er,p}$

$J_{er,p}$ models the ER membrane Ca^{2+} ATPase pump, also referred to as SERCA:

$$J_{er,p} = V_{er,p}[Ca^{2+}]_i^2/([Ca^{2+}]_i^2 + K_{er,p}^2) \tag{41}$$

$V_{er,p}$ was a constant (see section 7), and dictates the pump rate. $[Ca^{2+}]_i$ was the cytosol Ca^{2+} concentration, while $K_{er,p} = 0.15$ was the dissociation constant. $J_{er,p}$ begin to reach its maximum capacity at around $0.4\,\mu M$.

4.3.4 $J_{m,in}$

This flux was due to voltage activated Ca^{2+} channels through the plasma membrane from extracellular space into cytosol (L-type channels). As stated in section 4.1 this current was either modeled as a constant, or as: $J_{m,in} = Ai_{Ca}/z_{Ca}F$ Where A is the area of the cell in cm^2, i_{Ca} was the current into the cell in $\mu A\,cm^{-2}$ while F was Faraday's constant. z_{Ca} was the valency of Ca^{2+}.

4.3.5 $J_{m,NaCa}$

$J_{m,NaCa}$ was the Na^+/Ca^{2+} exchanger which forces Ca^{2+} from the cytosol into extracellular space:

$$J_{m,NaCa} = V_{m,NaCa}[Ca^{2+}]_i^4/([Ca^{2+}]_i^4 + K_{m,NaCa}^4) \tag{42}$$

$V_{m,NaCa}$ was the pump rate specific for the Ca^{2+}/Na^+ exchanger, the dissociation constant $K_{m,NaCa} = 0.9$ and a Hill coefficient was 4. $J_{m,NaCa}$ had low sensitivity but high max capacity as described in figure 7.

4.3.6 $J_{m,p}$

The plasma membrane Ca^{2+} ATPase pump forces Ca^{2+} from the cytosol into extracellular space. It had a Hill coefficient of 2, and $K_{m,p} = 0.3$:

$$J_{m,p} = V_{m,p}[Ca^{2+}]_i^2/([Ca^{2+}]_i^2 + K_{m,p}^2) \tag{43}$$

As indicated by figure 7 it had high sensitivity but low max capacity.

4.4 External input

Two different external input signals were used to drive the model, the $IP3$ concentration in the cytosol, and the input current i_{input} which depolarize the cell. When gonadotropic cells are stimulated with GnRH hormone they will eventually produce IP3 as part of the GnRH signaling transduction pathway [18]. GnRH will also inactivate certain K^+ ion channels, which will in turn depolarize the cell [18]. The exact phenomena which inactivates K^+ ion channels is not known [18]. We did not model these processes, but just assumed that the $IP3$ concentration increased and that the cell was depolarized with i_{input} after some time. The $IP3$ level was modeled as either a step function or as exponentially increasing. The exponential function was only used in a few cases in order to reproduce selected findings in the LR model. In most of the simulations (and

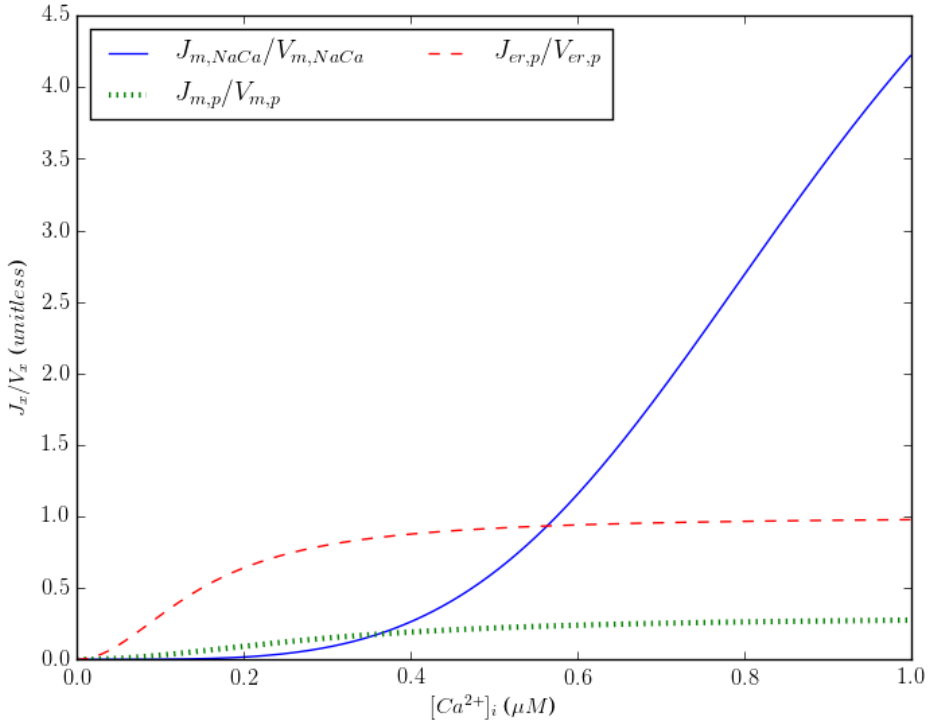

Figure 7: The figure shows how the Ca^{2+} ATPase ER membrane pump, Ca^{2+}/Na^{+} plasma membrane exchanger and the Ca^{2+} ATPase plasma membrane pump depends on $[Ca^{2+}]_i$. Equation 41, 42 and 43 shows how they are modeled.

unless otherwise specified) the step function was used. The step function was simply:

$$IP3 = \begin{cases} IP3_{basal} & \text{if } t < t_{input} \\ IP3_{input} & \text{if } t \geq t_{input} \end{cases}$$

Where $IP3_{basal}$ was the basal value of $IP3$, t_{input} was the time when the function changes and t was time. The exponential model was:

$$IP3 = \begin{cases} IP3_{basal} & \text{if } t < t_{input} \\ IP3_{input} + (IP3_{basal} - IP3_{input})e^{-(t-t_{input})/\tau_{IP3}} & \text{if } t \geq t_{input} \end{cases}$$

where

$$\tau_{IP3} = 60\Gamma(IP3_{input}, 0.6, 0.01)$$

The function $\Gamma(x, y, z)$ is defined by equation 34. When we later refer to the $IP3$ value we refer to the $IP3_{input}$ for simplicity. The input current were simply:

$$i_{input} = \begin{cases} 0 & \text{if } t < t_{depolarize} \\ i_{input} & \text{if } t \geq t_{depolarize} \end{cases}$$

Where $i_{depolarize}$ was the constant current that depolarized the cell, and $t_{depolarize}$ was the onset of the current. when we refer to i_{input} in our results we refer to $t_{depolarize}$.

4.5 Computer implementation

4.5.1 Programming language

The model was implemented using Python. Python was chosen since it has an intuitive syntax, is well supported and handles all memory allocation [23]. In short, using Python saved development time. The system of ordinary differential equations was solved using scipy.integrate.odeint. This function is based on LSODA, which is part of the FORTRAN library odepack [24]. LSODA is an adaptive solver, and automatically switches between stiff and non-stiff solver routines [22]. The code was divided into five blocks: cell_class, kinetic_schemes, new_parameters, derivative_call and the main script. Firstly, a cell is created by loading the cell_class in the main_script. The cell_class takes only two crucial parameters, the simulation time, and the time step size. When the cell_class is created, it loads a copy of all the relevant parameters from the new_parameters (table 2 and 1 in the appendix) document as a Python dictionary assigned to the specific cell. the cell_class then calculates the relationship between i_{Ca} and $J_{m,in}$, based on the diameter of the cell. After the cell is initialized, all the parameters can be explicitly changed through the main_script, making it easy to adjust values. When all initial values and other parameters are set, the cell_class function solve_system must be called through the main script. The solve_system function loads the integrate_odeint function, which take three parameters. The first parameter being the functions to be solved (see appendix), the initial conditions and a vector containing the time points we want a solution for. The function to be solved is defined in derivative_call. derivative_call also gets various function values, not dependent on time, from the kinetic_schemes. Finally the solution provided by scipy.integrate.odeint is saved as a part of the cell parameters, and can easily be called and plotted from the main_script. Figure 8 depicts this scheme, while figure 9 shows how the cell_class is used from the main_script. Of course the system of differential equations could have been solved without using Python objects, however dividing the code into separate parts most likely saved development time by making it easier to handle.

4.5.2 Implementation of the equations for L-type Ca^{2+}-channel activation

The equation 30 was rewritten when used in our simulations. This form has been used before by Halnes *et al.* [6]. We introduced Z which we defined as:

$$Z = z_x FV/RT \tag{44}$$

which contained the same parameters as in equation 30. We see that when $Z = 0$ the original equation 30 is not defined, which motivated us to use a rewritten form. We use the Z notation with the original equation:

$$i_{Ca} = P_{Ca} m^2 z_{Ca} FZ \frac{[Ca^{2+}]_i - [Ca^{2+}]_o e^{-Z}}{1 - e^{-Z}} 10^{-3}$$

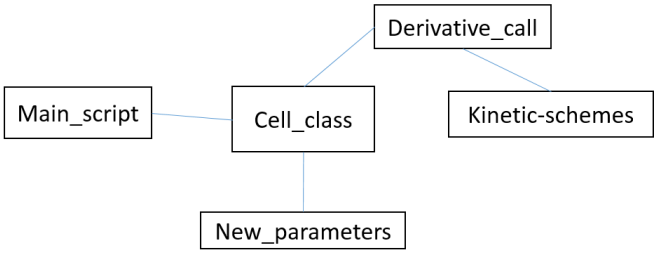

Figure 8: The cell_class is called through the main_script, and the model parameters are initialized through new_parameters. The solve_system function calls the deriative_call, which again loads various kinetic functions.

```
#Calling cell class
cell = Cell_class.Cell(50, 0.00001)

#Changing default parameters
cell.params['L_current_ON'] = True
cell.params['IP3_inject'] =  3
cell.params['Current_input_time'] = 60
cell.params['voltage_pump'] = -6

cell.set_diameter(20)

#Solving the system
cell.solve_system()
#plotting returned vectors
plt.plot(cell.time, cell.params['C_i'])
```

Figure 9: Typical usage of the cell_class through the main script. When the cell is created, the simulation time and time iteration step length is decided. The default parameters are then tuned as preferred, while the cell diameter is set. Finally the solve_system function is called, storing the solution as vectors. The solution can then easily be plotted.

We set:

$$G(V_m, [Ca^{2+}]_i, [Ca^{2+}]_o) = z_{Ca}FZ\frac{[Ca^{2+}]_i - [Ca^{2+}]_o e^{-Z}}{1 - e^{-Z}}$$

Which we can rewrite:

$$= z_{Ca}F\left(\frac{Z[Ca^{2+}]_i}{1 - e^{-Z}} - \frac{Z[Ca^{2+}]_o e^{-Z}}{1 - e^{-Z}}\right)$$

$$= z_{Ca}F\left(\frac{Z[Ca^{2+}]_i}{1 - e^{-Z}} - \frac{Z[Ca^{2+}]_o}{e^{Z} - 1}\right)$$

$$= z_{Ca}F\left(\frac{-Z[Ca^{2+}]_i}{e^{-Z} - 1} - \frac{Z[Ca^{2+}]_o}{e^{Z} - 1}\right)$$

And we introduced:

$$\xi(Z) = \begin{cases} 1 - Z/2 & |Z| < 10^{-4} \\ \frac{Z}{e^{Z}-1} & |Z| > 10^{4} \end{cases}$$

Where the term $1 - Z/2$ was the Taylor expansion of $\frac{Z}{e^Z-1}$ expanded around $Z = 0$. It containd the 0th and 1st term of the series. We now replace our $\xi(Z)$ with $\frac{Z}{e^Z-1}$ term in the original GHK equation:

$$G(V_m, [Ca^{2+}]_i, [Ca^{2+}]_o) = z_{Ca}F\left(\xi(-Z)[Ca^{2+}]_i - \xi(Z)[Ca^{2+}]_o\right) \quad (45)$$

which is defined for all Z. By using the rewritten form we reduced the chance running into computational errors when simulating the cell.

4.5.3 Implementation of the LR module

In the original LR article the equations governing the Ca^{2+} concentration in ER and cytosol were rewritten. This rewritten form was used to make the numerical calculations more accurate [10]. We also used this rewritten form in our simulations. The original rewritten form was also independent of the volume. In our case, when introducing Ca^{2+} through L-type channels the volume of the cell must be chosen as to determine how much the Ca^{2+} flux changes the concentrations (see table 2). We set $[Ca^{2+}]_{er} = C_{er}$ and $[Ca^{2+}]_i = C_i$ for simplicity. Equation 19 and 20 was first divided by P_{leak} :

$$\frac{V_i}{P_{ip3r}f_i}\frac{dC_i}{dt} = (P_{leak} + P_{ip3r}O)(C_{er} - C_i)/P_{ip3r} - J_{er,p}/P_{ip3r} + (J_{m,in} - J_{m,out})/P_{ip3r} \quad (46)$$

$$\frac{V_{er}}{P_{ip3r}f_{er}}\frac{dC_{er}}{dt} = -(P_{leak} + P_{ip3r}O)(C_{er} - C_i)/P_{ip3r} + J_{er,p}/P_{ip3r} \quad (47)$$

We now introduced:

$$\lambda = V_i/P_{ip3r}f_i \quad (48)$$

So our equation governing C_i became:

$$\lambda\frac{dC_i}{dt} = (P_{leak}/P_{ip3r} + O)(C_{er} - C_i) - J_{er,p}/P_{ip3r} + (J_{m,in} - J_{m,out})/P_{ip3r} \quad (49)$$

We also introduced the parameter $C_T = C_i + \sigma_{er}C_{er}$. We can use the distributive property of derivatives, and the fact that σ_{er} was a constant:

$$\frac{dC_T}{dt} = \frac{d(C_i + \sigma_{er}C_{er})}{dt} = \frac{dC_i}{dt} + \sigma_{er}\frac{dC_{er}}{dt}$$

We scaled our equation with λ:

$$\lambda\frac{dC_T}{dt} = \lambda\frac{dC_i}{dt} + \lambda\sigma_{er}\frac{dC_{er}}{dt}$$

Using $\lambda\sigma_{er}$ helped us:

$$\lambda\sigma_{er}\frac{dC_{er}}{dt} = \frac{V_iV_{er}f_i}{P_{ip3r}f_iV_if_{er}}\frac{dC_{er}}{dt}$$

$$\lambda\sigma_{er}\frac{dC_{er}}{dt} = \frac{V_{er}}{P_{ip3r}f_{er}}\frac{dC_{er}}{dt}$$

We noticed that $\lambda\frac{dC_i}{dt}$ was of course the same as the right hand side of equation 46, and that $\lambda\sigma_{er}\frac{dC_{er}}{dt}$ was the same as right hand side of equation 47:

$$\lambda\frac{dC_T}{dt} = (P_{leak} + P_{ip3r}O)(C_{er} - C_i)/P_{ip3r} - J_{er,p}/P_{ip3r} + (J_{m,in} - J_{m,out})/P_{ip3r} +$$

$$-(P_{leak} + P_{ip3r}O)(C_{er} - C_i)/P_{ip3r} + J_{er,p}/P_{ip3r}$$

$$\lambda\frac{dC_T}{dt} = (J_{m,in} - J_{m,out})/P_{ip3r}$$

Finally, the Ca^{2+} fluxes out of the plasma membrane were rewritten so that:

$$J_x = j_x\epsilon P_{ip3r} \tag{50}$$

Where $\epsilon = A_{pl}/A_{er}$. We chose to rewrite the equations slightly:

$$\lambda\frac{dC_T}{dt} = -J_{m,out}/P_{ip3r} + J_{m,in}/P_{ip3r}$$

$$\frac{dC_T}{dt} = -j_{m,out}\epsilon/\lambda + J_{m,in}/(\lambda P_{ip3r})$$

which is:

$$\frac{dC_T}{dt} = -j_{m,out}\epsilon/\lambda + J_{m,in}f_i/V_i$$

. We let

$$J_{er,p}/P_{ip3r} = j_{er,p} \tag{51}$$

and $P_{leak} = p_{leak}/P_{ip3r}$. The final equations governing Ca^{2+} concentrations were then:

$$\frac{d[Ca^{2+}]_i}{dt} = ((p_{leak} + O)([Ca^{2+}]_{er} - [Ca^{2+}]_i) - j_{er,p})/\lambda$$
$$- (j_{m,p} + j_{m,Na/Ca})\epsilon/\lambda + J_{m,in}f_i/V_i \tag{52}$$

$$\frac{[Ca^{2+}]_T}{dt} = -(j_{m,p} + j_{m,Na/Ca})\epsilon/\lambda + J_{m,in}f_i/V_i \tag{53}$$

By setting $j_{m,out} = j_{m,p} + j_{m,Na/Ca}$. We also changed back to the original notation for concentrations. We have that $O = a_\infty b_\infty d_\infty h$. We see that $J_{m,in}$ has units $\mu\text{mol}\,\text{s}^{-1}$ when V_i (and V_{er}) has units in liters. For each time iteration, $[Ca^{2+}]_{er}$ is needed in order to determine various kinetic functions or pump activity. $[Ca^{2+}]_{er}$ is easily obtained by just rewriting the definition of $[Ca^{2+}]_T$: $[Ca^{2+}]_{er} = ([Ca^{2+}]_T - [Ca^{2+}]_i)/\sigma_{er}$. Notice, that in our model $\lambda = V_i/P_{ip3r}f_i$ was assumed constant for all V_i. So that changing the volume V_i automatically changed the P_{ip3r} conductivity. ϵ is also assumed constant for all V_i.

5 Results

5.1 the ER module

5.1.1 Reproducing the IP3 channel opening in the LR module

When solving the equations described in the article by Li *et al.* [10], we did not manage to reproduce the system dynamics reported in this article. Seemingly, there was a mismatch between the equations that we had implemented and the equations that had been solved in the LR article.

Further exploration revealed that the source of this mismatch was in the channel opening kinetics (plotted on page 59 LR[10]). As it turned out, our model of of 'O' was not in agreement with the original model of the opening kinetics. O is the opening probability of J_{IP3} which is explained in section 4.3. Knowing that the channel opening O depended on four distinct channels ($O = a_\infty b_\infty d_\infty h$), each channel was plotted independently depending on $[Ca^{2+}]_i$. Figure 10 shows how h_∞ depended on $IP3$, $[Ca^{2+}]_{er}$ and $[Ca^{2+}]_i$, while figure 11 shows the gating variable dependency on the same parameters. As a_∞ had a peculiar jump when $[Ca^{2+}]_i = 0.4$ µM it seemed reasonable to assume that the kinetic schemes expressing this opening variable was wrong.

After closer examination of a_∞ we concluded that the expression for k_a (which a_∞ depends on) most likely had a missing parenthesis in the original LR [11]. The original equation with missing parenthesis was:

$$k_a = \left(0.16\frac{10}{10 + [Ca^{2+}]_{er}}\right)\left\{\left(1 + \frac{IP3}{0.2 + IP3}\right)\left(\frac{0.15^2}{0.15^2 + (IP3 - 0.25)^2}\right)\right\}$$

The equation for k_a was found to be:

$$k_a = \left(0.16\frac{10}{10 + [Ca^{2+}]_{er}}\right)\left\{1 + \left(\frac{IP3}{0.2 + IP3}\right)\left(\frac{0.15^2}{0.15^2 + (IP3 - 0.25)^2}\right)\right\}$$

. When we used this equation, the channel opening depending on $IP3$, $[Ca^{2+}]_{er}$ and $[Ca^{2+}]_i$ as in LR [10] was reproduced. The opening probability is shown in figure 12.

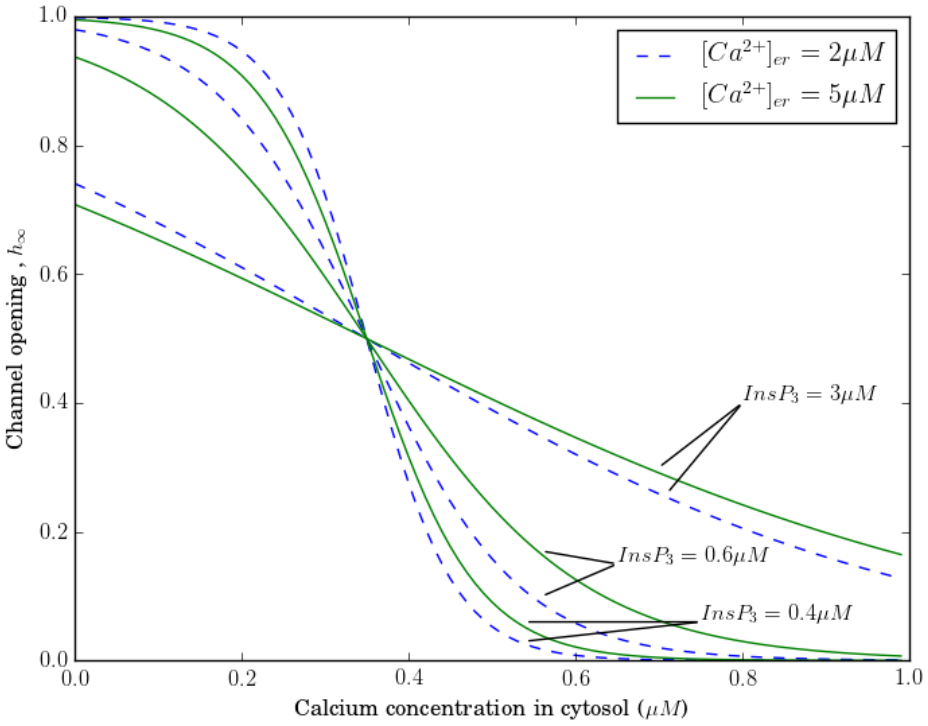

Figure 10: Channel opening h_∞ depending on $IP3$, $[Ca^{2+}]_{er}$ and $[Ca^{2+}]_i$.

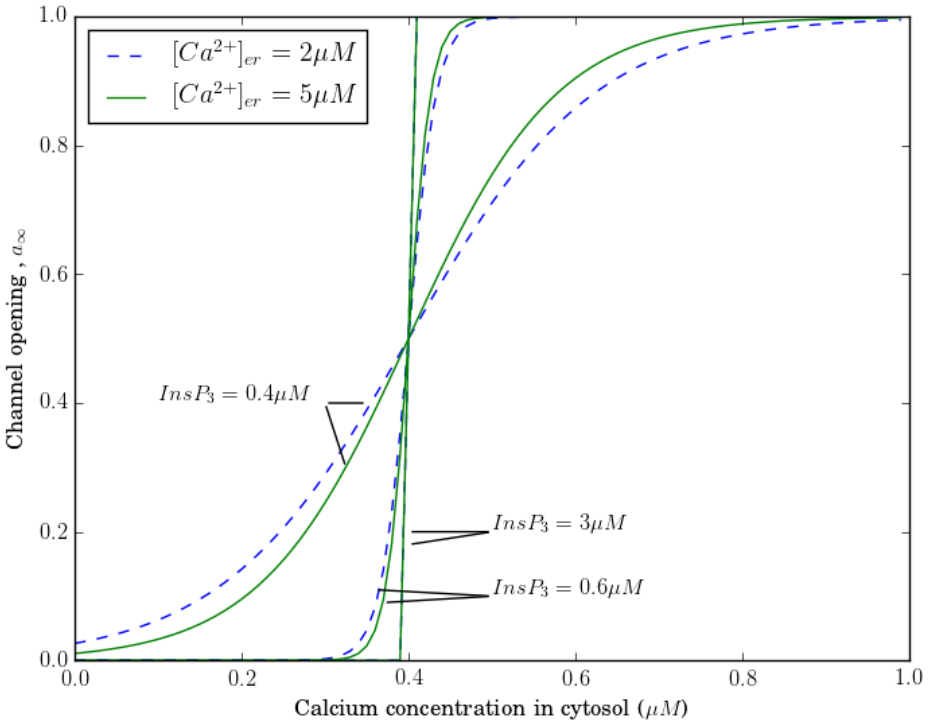

Figure 11: Channel opening a_∞ depending on $IP3$, $[Ca^{2+}]_{er}$ and $[Ca^{2+}]_i$, as originally described in LR [11]. When $[Ca^{2+}]_i$ is 0.4 µM, a_∞ changes abruptly when $IP3$ is over 0.4 µM.

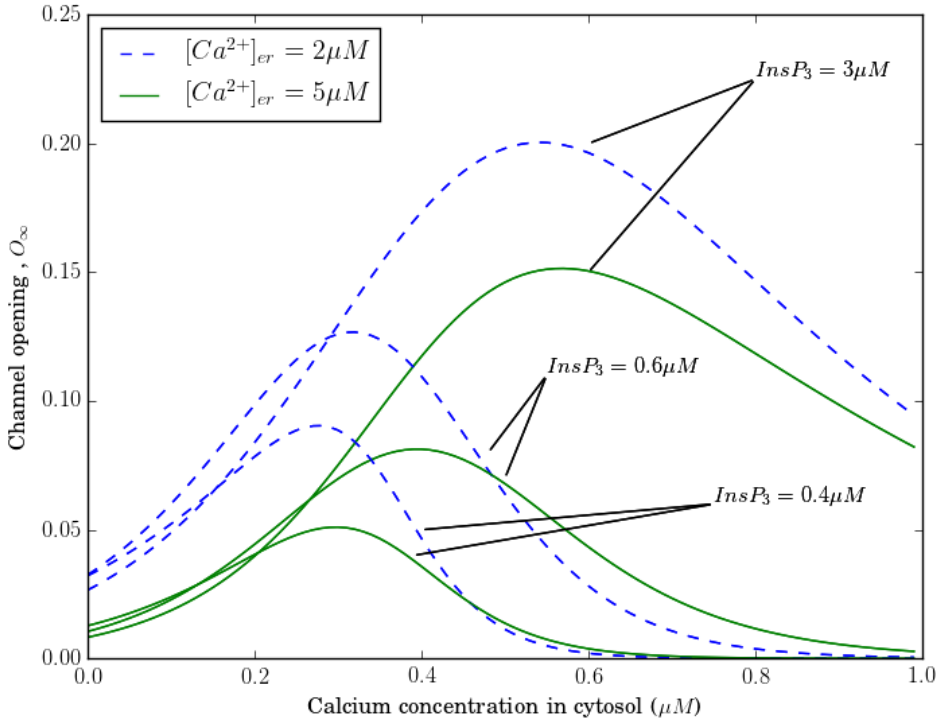

Figure 12: Channel opening O_∞ depending on $IP3$, $[Ca^{2+}]_{er}$ and $[Ca^{2+}]_i$

5.1.2 IP3 induced Ca^{2+} release

In this chapter we will study the ER and cytosol Ca^{2+} dynamics obtained with the LR module, but with the corrected expression for k_a as described in the previous section. In table 2 in the appendix we have listed all relevant parameters used in our simulation.

Figure 13 shows how Ca^{2+} concentration changed with varying input of cytosol $IP3$ concentration. $IP3$ will activate the J_{IP3} ER membrane current, and release Ca^{2+} into the cytosol. Figure 13A, 13B and 13C shows the Ca^{2+} oscillations with $J_{m,in} = 0$ so that no Ca^{2+} flows into the cell from extracellular space. Figure 13A shows Ca^{2+} oscillations when the IP3 was exponentially increased from the basel level to $IP3 = 0.4$µM, which is explained in section 4.4. Figure 13B shows the Ca^{2+} response with $IP3 = 1.425$ µM, while figure 13C shows the Ca^{2+} response with $IP3 = 3$ µM.

Figure 13D, 13E, 13F shows the Ca^{2+} response when $j_{m,in}$ was set to 0.175 µM (see chapter 7.2 regarding units), so that Ca^{2+} flows into the cell from extracellular space. The simulations depicted in figure 13D, 13E, 13F have the same IP3 configurations as the simulations depicted in 13A, 13B and 13C respectively.

Figure 13A-F represents the finalized reproduction of the Ca^{2+} oscillation as were originally presented by LR [10]. In our simulation, we noticed some minor differences from LR. The simulation with $IP3 = 0.4$µM and $j_{m,in} = 0$ (figure 13 in our case had four Ca^{2+} spikes, while in the original paper it had five. In the case of $IP3 = 1.425$µM, after the Ca^{2+} plateau we only noticed two major Ca^{2+} oscillations (figure 13B, after $t = 100$s), while in the original paper there are 4 small oscillations after the prolonged Ca^{2+} plateau. Otherwise, our simulation produced about the same result as was done in the original LR article [10]. We decided that our simulations reproduced the original results satisfyingly, and kept this as our final model of the Ca^{2+} dynamics in the cytosol and ER, namely the LR module.

Figure 14 represents the same simulations as in figure 13, only here we have plotted $[Ca^{2+}]_{er}$. Figure 14A represent ER concentration in the same simulation as figure 13A, while figure 14B represent free $[Ca^{2+}]_{er}$ in the same simulation as plotted in 13 and so forth. We see how the channel opening O dependency on $[Ca^{2+}]_{er}$, $[Ca^{2+}]_i$ and $IP3$ dictated the Ca^{2+} fluctuations as described by 12. At $IP3 = 0.4$µM as described by 13A and 14A we see how the Ca^{2+} fluctuated between ER and cytosol. With low $[Ca^{2+}]_i$ and high $[Ca^{2+}]_{er}$ the channels activated and released Ca^{2+} through ER into cytosol. This raised $[Ca^{2+}]_i$, which then caused the channel to inactivate as described by figure 12 and then repeating the process. Eventually the Ca^{2+} in the ER is depleted. When $IP3 = 3$ µM as shown in figure 13C and figure 14C we noticed however that $[Ca^{2+}]_i$ never manages to inactivate the channel opening O in the range between 0 and 1 µM, which explains why there were no oscillations when $IP3 = 3$µM.

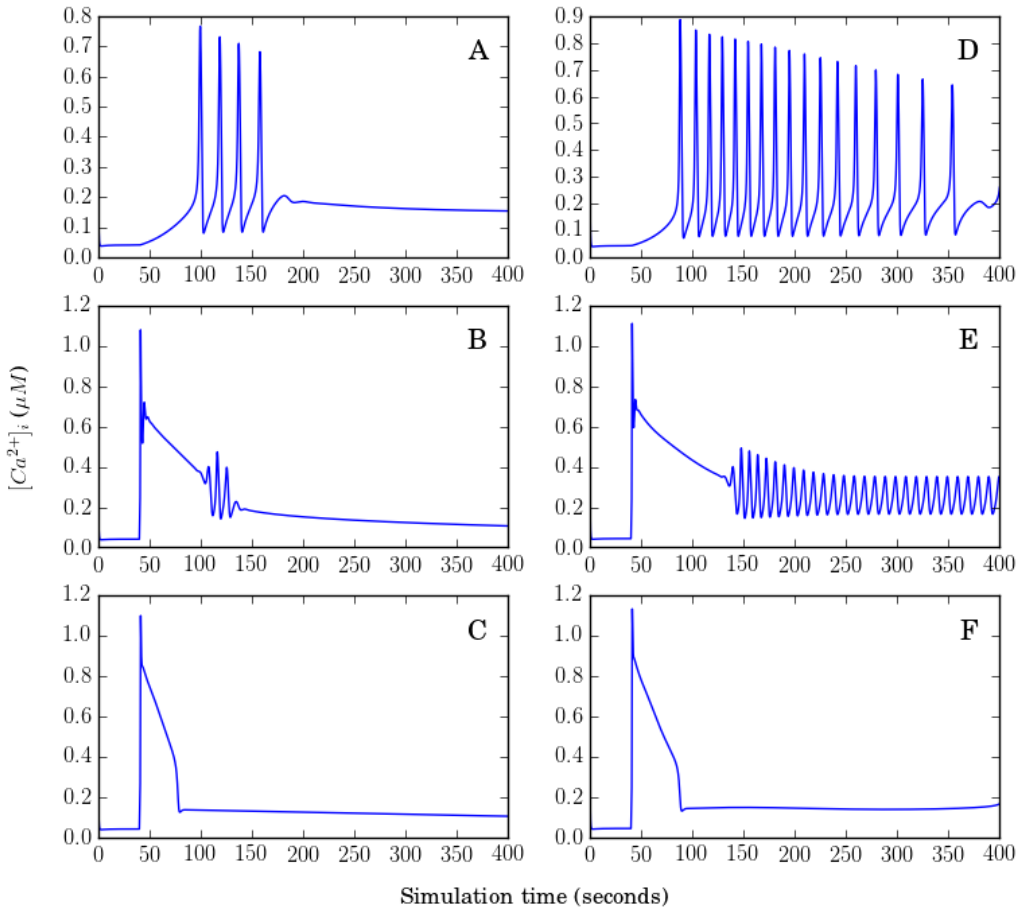

Figure 13: Original LR reproduced, with model parameters as in table 2. $IP3$ concentration is changed after 40 seconds. In figure A, B and C $J_{m,in} = 0$, while in figure D, E and F $j_{m,in} = 0.175$ µM. In A and D, Cytosol $IP3$ was raised exponentially from the basal value 0.03 µM to 0.4 µM (see section 4.4). In figure B and E $IP3$ is raised instantly from the basal value to 1.425 µM. In figure C and F $IP3$ was instantly raised to 3 µM.

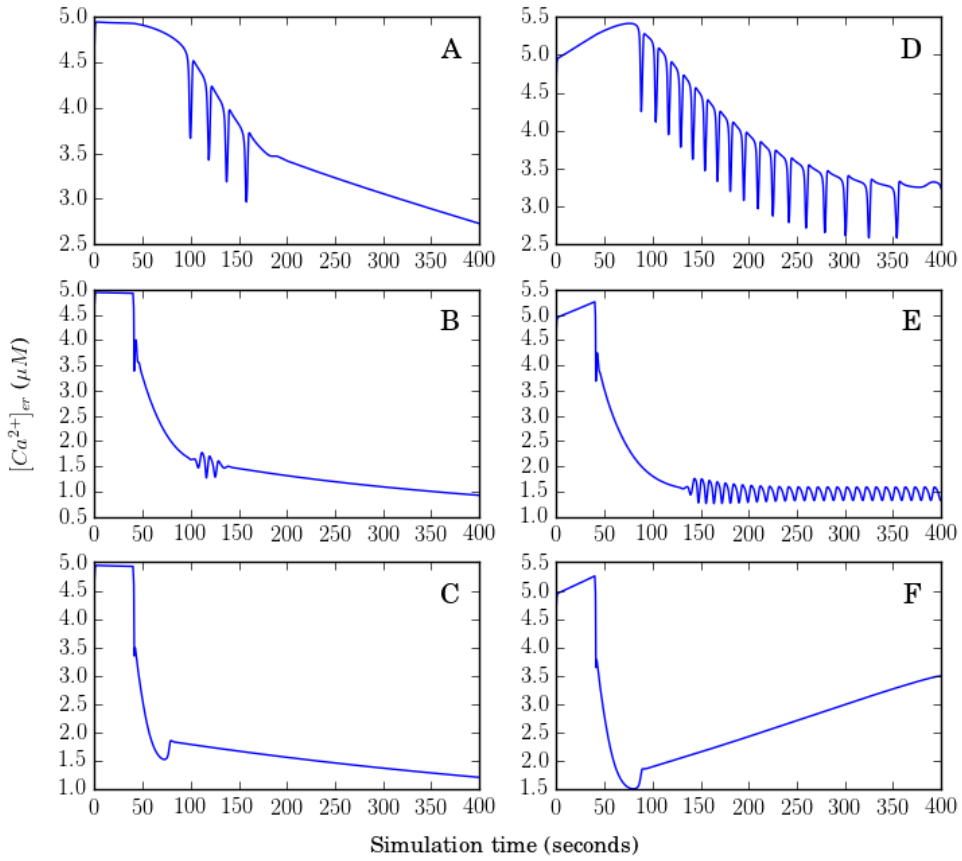

Figure 14: The respective $[Ca^{2+}]_{er}$ for each simulation in figure 13. Notice Ca^{2+} oscillating between ER and cytosol at low $IP3$ values (fig A, B, D and E). Ca^{2+} continuously deplete through the plasma membrane.

5.2 FD module: A model for Ca^{2+} influx through the plasma membrane

After the $IP3$ activated Ca^{2+} release one often experimentally record that the plasma membrane depolarize and start to fire action potentials [18]. It is believed that the second part of the biphasic response shown in figure 1 in section 1 observed is due to L-type channels. These channels are voltage activated and will release Ca^{2+} into the cell during an action potential.

In this section we present a model for the plasma membrane, the FD module, which contain action potential generating Na^+ and K^+ channels, as well as the L-type Ca^{2+} channel. We used this to investigate the L-type channel's impact on the cytosol Ca^{2+} concentration. In order to study the plasma-membrane model in isolation, we first considered a simplified scenario where all fluxes over the ER membrane were set to zero, so that only the plasma membrane currents and Ca^{+2} fluxes were present. The ER fluxes J_{IP3}, $J_{er,p}$ and $J_{passive}$ were set to zero (see section 4.3 for description). This was done by setting $p_{er,l} = 0$, $v_{er,p} = 0$ and $O = 0$, otherwise the model was implemented as described in the appendix. Now, Ca^{2+} in cytosol was only dependent on the $J_{m,Na/Ca}$ due to the Na^+/Ca^{2+} exchanger, the plasma membrane Ca^{2+} ATPase pump $J_{m,p}$ and of course $J_{m,in}$ due to L-type channels.

We made the cell fire action potentials by depolarizing the plasma membrane with an artificial input current. The action potentials were created through Na^+/K^+ channel dynamics. As we will see, the L-type voltage activated Ca^{2+} channels not only impact the Ca^{2+} flux through the plasma membrane, but will also alter the of shape the action potential.

5.2.1 The action potential produced by Na^+ and K^+ channels

To explore the membrane dynamics in a systematic way, we first made simulations on a reduced model, which only contained the Na^+ and K^+ channels.

Figure 15 A show how the K^+ and Na^+ channels as described in section 4.2.1 generated action potentials. Through a series of simulations, the Na^+ conductance $\bar{g}_{Na}$ was tuned as to get a reasonable amplitude, while the K^+ conductance $\bar{g}_K$ was tuned to get a reasonable hyperpolarizing between action potentials. Since the L-type channels also alters the action potential, we did not focus on getting an exact reproduction of the recorded action potentials but rather the qualitative shape. The shape of the action potential was based on recordings of gonadotropes in medaka stimulated by GnRH (Kjetil Hodne, personal communication, February, 2016). The simulation in figure 15 shows a action potential with conductances from table 1 in the appendix.

The shape of the action potential is also dependent on temperature. With lower temperatures the kinetics of the gating variables becomes slower, and so the action potential width becomes broader. In the Halnes model [6], from which we took our model of Na^+ and K^+ channels, the width of the action potential were shorter than what has been experimentally recorded in gonadotropes in medaka durign GnRH stimulation. Experimental recordings shows that AP in gonadotropic medaka has a width of about 5 ms (Kjetil Hodne, personal communication, February, 2016). In the Halnes model, the temperature was set to 36 °C [6]. We tuned the temperature to 34 °C so that the width became 4 ms, knowing that the L-type channel could broaden the AP. 34 °C however is

not physically correct since the temperature when the biphasic and monophasic Ca^{2+} response were recorded was about 25 - 28 °C [18].

By setting the input current i_{input} to approximately 3.5904 µA cm^{-2} we managed to obtain an firing frequency of about 2 Hz, which is about the AP firing frequency of gonadotropic medaka when stimulated by GnRH [18].

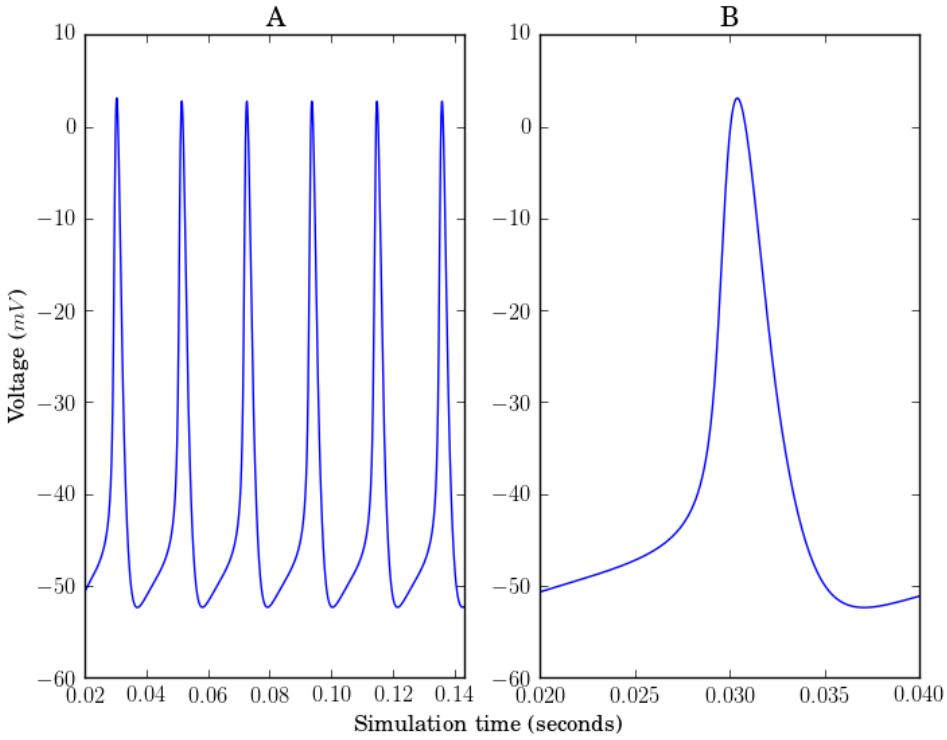

Figure 15: Figure A shows K^+ and Na^+ channels generating action potentials where $T = 34$°C. Current input of 5 µA cm^{-2}. Figure B shows a closer look at a single action potential. K^+ and Na^+ channels created the typical AP observed in medaka.

5.2.2 Influence of L-type Ca channels on action potential shape

Next, we studied how the AP shape was influenced when L-type Ca^{2+} channel was added to the system. Figure 16 shows the influence of the L-type channel on the action potential shape. As stated in the previous section, 5 ms is the typically observed action potential width of gonadotropic cells when stimulated with GnRH. We tuned P_{Ca} permeability to match this. The width of the action potential increased to 5 ms with a L-type permeability of 0.2 dam s^{-1}. The L-type channels also decreased the firing rate of the cell. Simulating for 10 seconds with a input current of 6 µA cm^{-2} and $[Ca^{2+}]_i$ locked at 0.1 µM, gave a firing frequency of 60.9 Hz without L-type channels. With $P_{Ca} = 0.2$ dam s^{-1} the frequency became 55.3 Hz. The frequency drop is most likely due to the broadening of the action potential. The action potential becomes wider and higher since Ca^{2+} flux depolarize the cell. We also checked if different $[Ca^{2+}]_i$ would change the firing frequency with $P_{Ca} = 0.2$ dam s^{-1}, but fixing $[Ca^{2+}]_i$ to 1 µM revealed no significant change. The temperature T_{Ca} which goes into equation 45 was set to 300 K, as this matches the temperature of the experimental recordings [18].

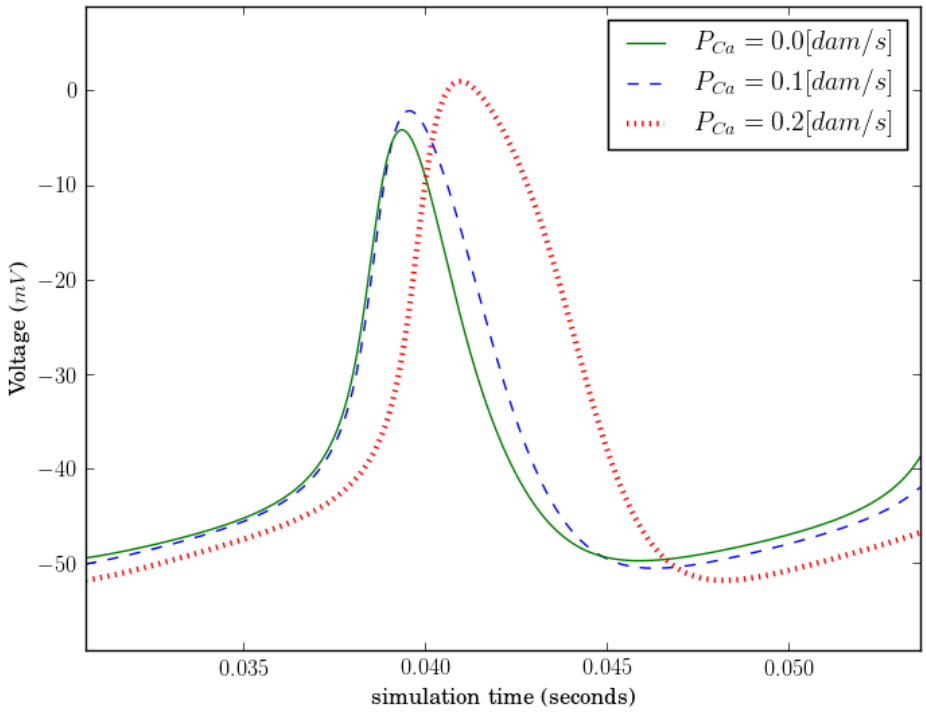

Figure 16: Action potential with same input current as in figure 15. L-type channels increased the amplitude with about 10 mV, while also increasing the width of the action potential to about 5 ms.

5.2.3 Cytosol Ca^{2+} dynamics due to L-type Ca^{2+} channel influx

Next, we explored the L-type channel influence on $[Ca^{2+}]_i$ in the simplified model, where the ER compartment was not included. Figure 17 shows the model responing to an input current which caused a firing rate of 2 Hz. Here, Ca^{2+} influx $J_{m,in}$ to the cell was solely due to the L-type channels. Notice, when the cell fires action potentials the L-channels caused a change in $[Ca^{2+}]_i$ of about 50 nM per AP. From figure 17 we see that the Ca^{2+} dynamics due to $J_{m,in}$ and the Ca^{2+} dynamics of the LR module are of the same magnitude, which makes the influence of the L-type channel plausible. 50 nM increase in $[Ca^{2+}]$ per action potential has also been observed before [1], but in a different cell type.

Figure 18 shows how Ca^{2+} fluxes across the plasma membrane $J_{m,Na/Ca}$ increased as $[Ca^{2+}]_i$ went up, while $J_{m,p}$ stayed about the same. $J_{m,in}$ max was about 6×10^{-10} µmol s^{-1} which is about 100 times higher than $J_{m,Na/Ca}$ max. This is reasonable since $J_{m,in}$ only lasted for about 5 ms every half second while $J_{m,NaCa}$ was about its maximum in the time frame of one second. We also noticed that $J_{m,in}$ due to the L-type channel was active when the cell did not fire.

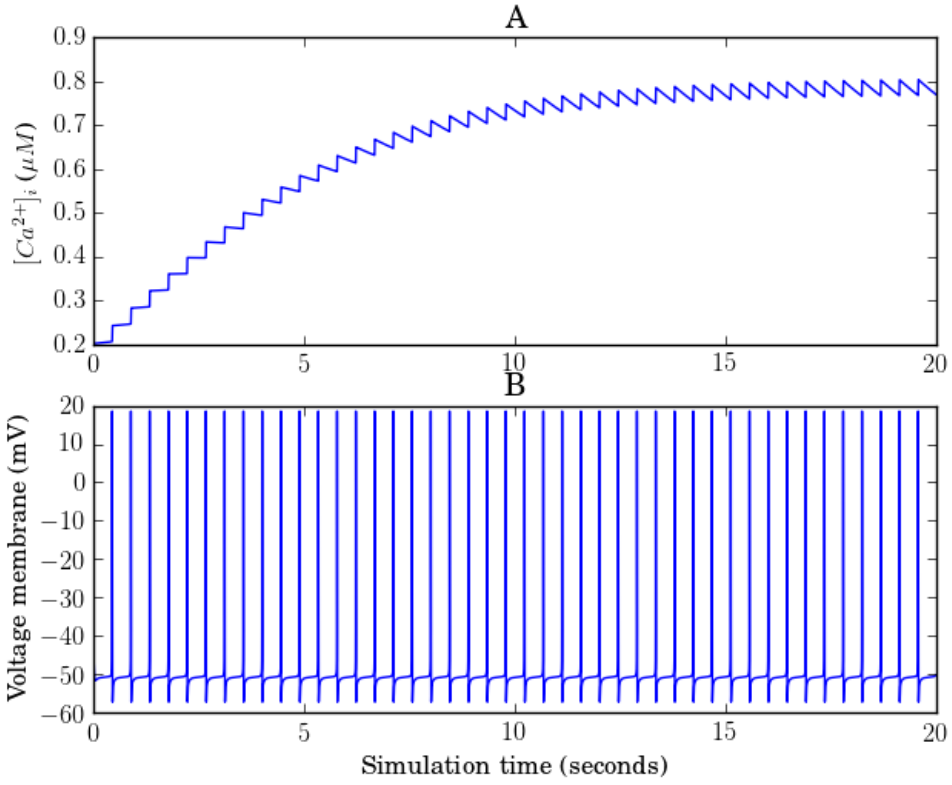

Figure 17: The figure A shows how the Ca^{2+} influx from the L-type channel changed $[Ca^{2+}]_i$ when ER was blocked. Figure B shows the cell hyperpolarize and fire action potentials when the current input was 3.5904 µA cm^{-2}.

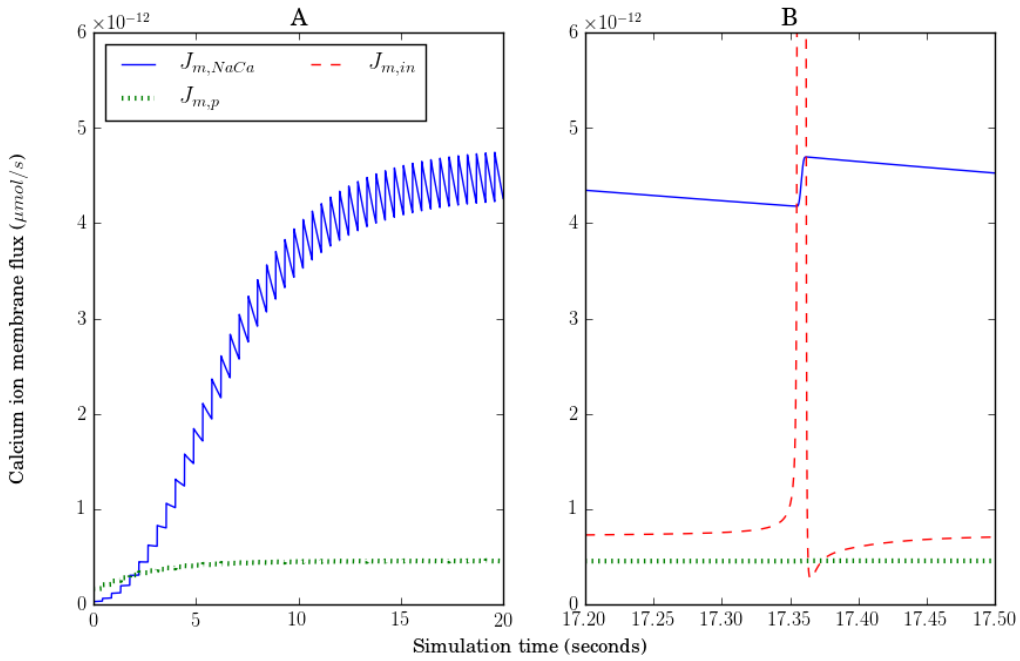

Figure 18: figure A and B shows $J_{m,in}$, $J_{m,NaCa}$ and $J_{m,p}$ with *ER* blocked and L-type channels activated. $J_{m,in}$ was excluded from figure A. Figure A shows how the $J_{m,NaCa}$ drastically increase with increased $[Ca^{2+}]_i$ (figure 17), while $J_{m,p}$ never exceeded 0.5×10^{-12} µmol s^{-1}. Figure B shows how $J_{m,in}$ rapidly increased at $t \approx 17.4$ s when an action potential occurred. $J_{m,in}$ was noticeably bigger than $J_{m,p}$ even when the cell did not fire. Notice $J_{m,in}$ reached about 6×10^{-10} µmol s^{-1} which is not shown in figure B.

5.3 A model of the biphasic response observed in gonandotropic cells

Our main goal was to produce the biphasic response as observed in medaka gonadotropic cells (see section 1). The biphasic response consists of two parts. The initial increase in $[Ca^{2+}]_i$ is believed to consist of Ca^{2+} released from ER [18], while the second increase is due to uptake of Ca^{2+} from extracellular space through L-type channels. In order to model this we used a combined model, which included both the LR module from section 5.1 and the FD module from section 5.2.

In results part 5.1.2, we observed that in the case of $IP3 = 3\mu M$ our model reproduced a similar monophasic response as was observed in med-aka, which is shown in figure 1 section 1. We therefore chose this as the $IP3$ input value as a part of our full simulation. Our $J_{m,in}$ was now due to our L-channel, implemented the same way as in section 5.2, but now the ER was naturally not blocked.

3 µM IP3 was inserted after 5 seconds, while the input current i_{input} was set to $3.5904\,\mu A\,cm^{-2}$ after 20, 35 and 60 seconds in three separate simulations. Figure 19 shows the three simulations. Firstly we see that free cytosol $[Ca^{2+}]_i$ increased at $t = 5s$ as Ca^{2+} was released from ER due to increased $IP3$ which opened $IP3$ dependent Ca^{2+} channels on the ER membrane. Figure 20 shows how the $[Ca^{2+}]_{er}$ decreased correspondingly. While $[Ca^{2+}]_{er}$ continued to deplete, cytosol Ca^{2+} then escaped into extracellular space through the Na^+/Ca^{2+} exchanger $J_{m,NaCa}$ and Ca^{2+} ATPase pump.

The cell shown in figure 19A started to depolarize and fire action potentials after 20 seconds, and as shown in section 5.2.3 these action potentials activated the L-type channels which released Ca^{2+} into the cytosol through the plasma membrane. Now the $[Ca^{2+}]_i$ started to increase slowly, and then began to stabilize at around 0.8 µM after about 100 seconds.

While $[Ca^{2+}]_i$ started to converge so did the $[Ca^{2+}]_{er}$, as shown in figure 20 A. This meant that the Ca^{2+} flux into ER were equal to the Ca^{2+} flux out of the ER, so that $J_{tot} = J_{IP3} + J_{passive} + J_{er,p} = 0$. The SERCA pump $J_{er,p}$ was noticeably only dependent on $[C^{2+}]_i$, while J_{IP3} and $J_{passive}$ were dependent on both $[C^{2+}]_i$ and $[C^{2+}]_{er}$. When $[C^{2+}]_i$ increased so did $J_{er,p}$ (SERCA pump). While this happened, the $[Ca^{2+}]_{er}$ started to increase. When $[Ca^{2+}]_{er}$ got bigger, so did the driving force of the J_{IP3} and $J_{passive}$. In the end, when $[Ca^{2+}]_{er}$ reached $\approx$ 2.5 µM and $[Ca^{2+}]_i$ was $\approx$ 0.8µM we had that $|J_{IP3} + J_{passive}| = |J_{er,p}|$ because of the increase of $[(C^{2+}]_{er} - [C^{2+}]_i)$.

We also simulated the cell in the case of depolarizing after 35 seconds as shown in figure 19B and 20B. The cell behaved much like in the situation of hyperpolarization after 20 seconds (fig. 19A and 20A), only that $[Ca^{2+}]_i$ was about 0.5 µM before the hyperpolarizing of the cell caused influx of Ca^{2+} through the L-type channels on the plasma membrane. This simulation somewhat resembled the biphasic $[Ca^{2+}]$ response observed in medaka [18].

Lastly, the simulation of hyperpolarization after 60 seconds is showed in figure 19C and 20C. We observed an interesting phenomenon at the start of the hyperpolarization: the increase of $[Ca^{2+}]_i$ not only happened because of $J_{m,in}$ due to L-type channels, but a release of Ca^{2+} from ER which is evident from figure 20C. This release is again explained by the opening variable O. Figure

12 showed that the channel opening peaks at $\approx$ 0.6µM, and so that increasing $[Ca^{2+}]_i$ actually increased the J_{IP3} pump-rate into the cytosol which caused a positive feedback. This positive feedback ends when $[Ca^{2+}]_i$ exceeded $\approx$ 0.6µM, and now J_{IP3} did decrease somewhat. Other factors may also explain the decline, such as $[Ca^{2+}]_{er}$ depleting and lowering the Ca^{2+} driving force over the membrane.

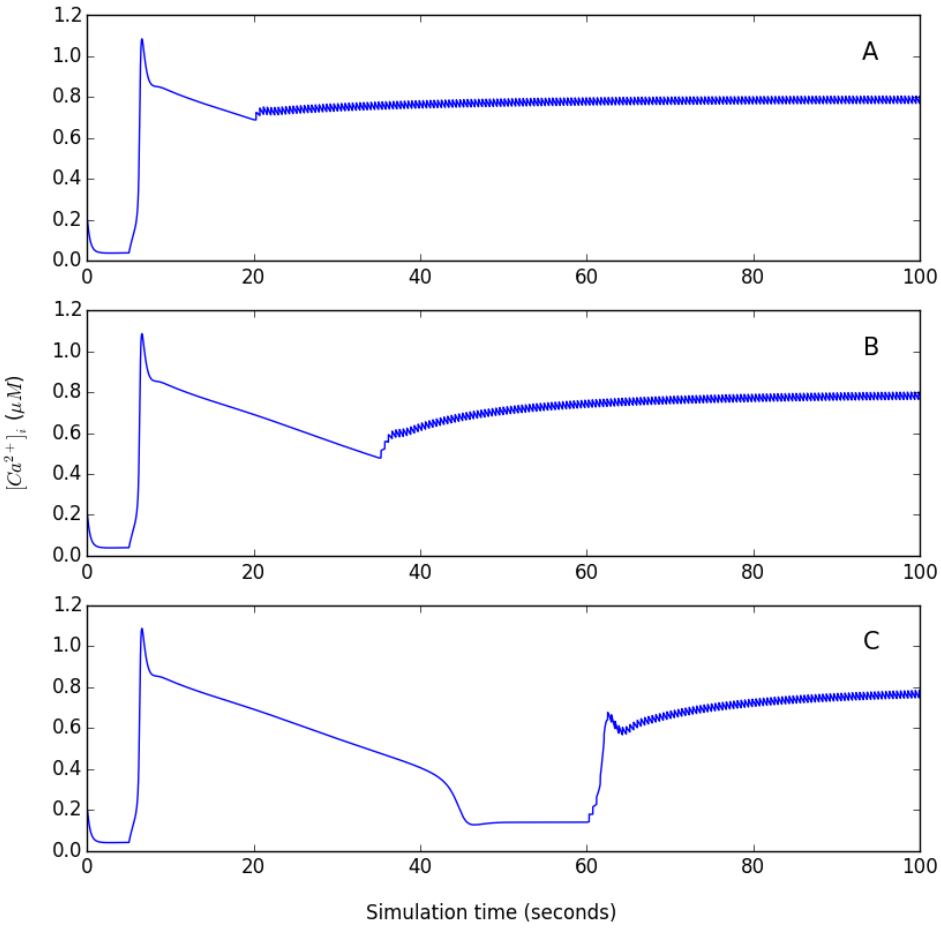

Figure 19: In A,B and C $IP3$ is raised to 3 µM after 5 seconds, as in figure 13C. In figure A extracellular Ca^{2+} is released into the cell through the L-type channel after 20 seconds when the cell begins to fire action potentials. In figure B the cell starts to fire after 35 seconds while in figure C after 60 seconds. $[Ca^{2+}]_i$ converge to 0.8 µM in A,B and C.

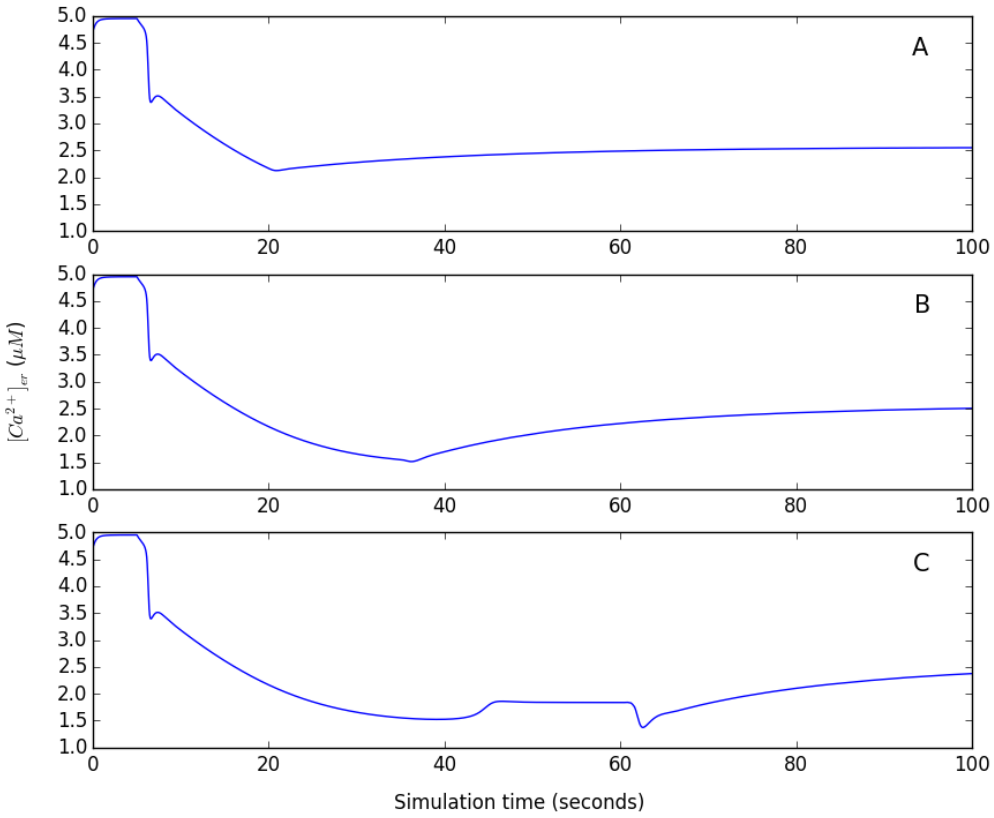

Figure 20: Figure A, B and C shows same simulation as in figure 19A, figure 19B and figure 19C respectively. Notice, in figure C there is a clear release of Ca^{2+} from ER after 60 seconds. In each case, the $[Ca^{2+}]_{er}$ converge to $\approx$ 2.5 µM.

5.3.1 Ca^{2+} accumulation in ER

Even though our model managed to reproduce the biphasic response reasonably well, we did however experience unwanted model behaviour. When the $IP3$ concentration was constantly at basal value (0.03 µM), and with constant influx of Ca^{2+} through the plasma membrane, the ER would accumulate Ca^{2+}. This is shown in figure 21A.

We will study this scenario by using the same model as in section 5.1.2 and with constant $j_{m,in} = 0.175$ µM. Since the $IP3$ value was constantly at 0.03 µM the model did not induce a Ca^{2+} release through J_{IP3}. To try to deal with this, we altered the passive leak mechanism over the ER membrane. The passive leak permeability has the form $p_{er,l}([Ca^{2+}]_{er} - [Ca^{2+}]_i)$, which means increasing $[Ca^{2+}]_{er}$ (while $[Ca^{2+}]_i$ is constant) increased the leak flux out of ER. The leak permeability $p_{er,l}$ was changed from the original LR value of 0.0005 to 0.02. At this level the Ca^{2+} did not accumulate drastically in the ER, while instead slowly converging to 5.4 µM, later dropping to 5.2 µM and after that repeating the same process as indicated by figure 21.

We did however decide not to include the altered leak permeability in the biphasic response simulation in section 5.3, as the cytosol Ca^{2+} showed undesired fluctuations as depicted in figure 21D.

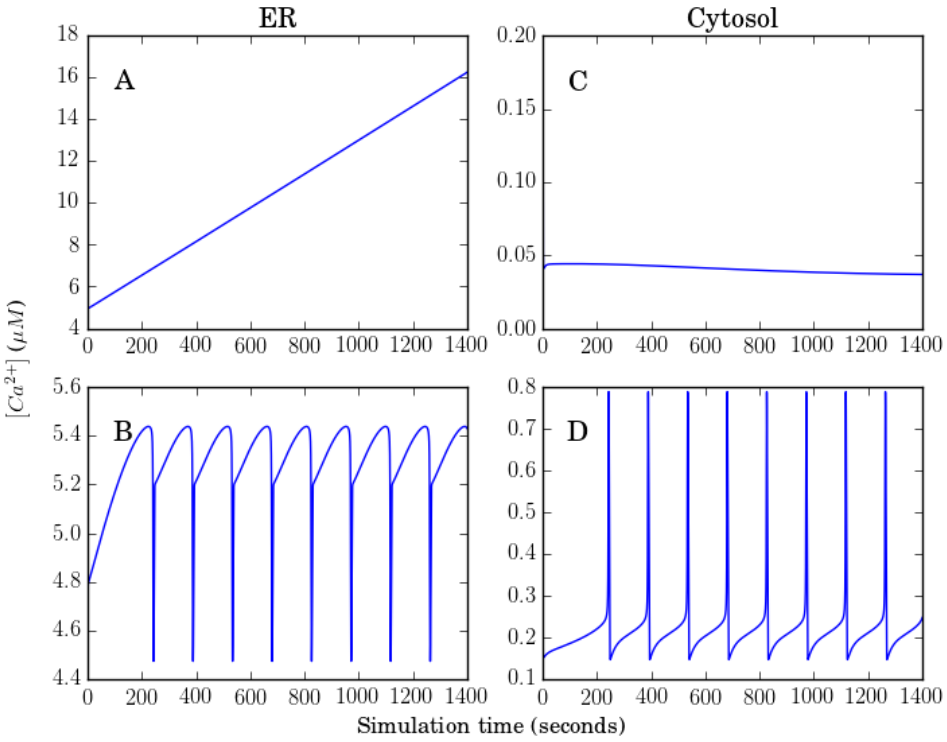

Figure 21: Figure A shows $[Ca^{2+}]_i$ while figure C shows $[Ca^{2+}]_{er}$ when the cell is simulated with ordinary LR parameters (see table 2), only now $j_{m,in} = 0.175$ µM and $IP3$ is always at basal value (0.03 µM). Figure B shows $[Ca^{2+}]_i$ and figure C shows $[Ca^{2+}]_{er}$ with the cell simulated with same parameters as in A and C, only now $p_{er,p} = 0.02$. Figure D shows undesired Ca^{2+} fluctuations which were introduced with the new leak permeability. Notice when $p_{er,p} = 0.02$ $[Ca^{2+}]_i$ is ≈ 0.2 µM even when Ca^{2+} is not released from ER, while in the case of $p_{er,p} = 0.0005$ (original value) $[Ca^{2+}]_i$ never exceeds 0.05 µM.

6 Discussion

In this thesis, we expanded a previous model for $IP3$ dependent Ca^{2+} release (LR module) in mammalian gonadotrope cells by adding additional voltage dependent mechanisms (FD module) on the plasma membrane. By combining these modules, we were able reproduce qualitative features of the biphasic Ca^{2+} response observed experimentally in gonadotope cells in medaka. In the next section, we will discuss how assumptions made could have affected the results and what could have been done differently.

6.1 Influx of Ca^{2+} through L-type channels

A part of reproducing the biphasic response observed in medaka was to show the L-type channel influence on $[Ca^{2+}]_i$. The influence produced by the L-type channel was in agreement with earlier observations [1], although earlier observations concerned a different cell type. Physical assumptions were made when employing the L-type channel.

For simplicity, we assumed no spatial dependencies in the intracellular ER and cytosol Ca^{2+} compartments, neither in extracellular space. In reality however, as Ca^{2+} enters a compartment the concentration will be higher close source of the influx. Eventually, as time goes by the Ca^{2+} becomes evenly distributed throughout the compartment due to Brownian motion. In our model, we assumed that Ca^{2+} spread out instantly. For example, when L-type channels are open on the plasma membrane, it is likely that the concentration closer to the plasma membrane is in reality higher than the median cytoplasmic concentration. The increased concentration could then alter the driving force of the L-type channels as dictated by the Goldman Hodgkin Katz current equation (see section 3.2.1for description). A possible way to improve the model would be adding spatial dependency on intracellular and extracellular Ca^{2+} through mathematical modeling of diffusion.

Not only did we assume the instant spread of Ca^{2+}, but we also assumed that the fraction of free Ca^{2+} was constant. This means that we assumed Ca^{2+} fluxes that changed the Ca^{2+} concentration of the ER and cytosol would instantly maintain the fraction of free Ca^{2+}. This was a very big simplification, as the fraction of free Ca^{2+} is in reality governed by various intracellular mechanisms, often modeled by chemical reaction[16]. A changed fraction of free Ca^{2+} would in turn also influence Ca^{2+} fluxes through the L-channels governed by the Goldman Hodgkin Katz current equation. In the case of L-type channels, it would be reasonable to employ the rapid buffer approximation [14], which more accurately models the free Ca^{2+} concentration close to the plasma membrane during Ca^{2+} influx from extracellular space.

The choice of the L-type channels permeability could also be questioned. The choice was based on qualitative change of the action potential. Indeed more emphasis could have been paid, for example compare permeability P_{Ca} with earlier work.

We would also emphasize that addressing the L-type influence on $[Ca^{2+}]_i$, and the internal kinetics, are two issues which could have been addressed separately. If the median $[Ca^{2+}]_i$ is only in the range of $0.1 - 1\mu M$, this means that the L-type Ca^{2+} release is much more influenced by itself than the internal concentration. This means that understanding the L-type contribution to $[Ca^{2+}]_i$

can be done without determining the intracellular long term kinetics, such as $IP3$ channel activation on the ER membrane.

Since the firing frequency of medaka is only 2 Hz, it is reasonable to believe that the Ca^{2+} influence by one action potential is not affected by other action potentials other than the fact that the median cytoplasmic Ca^{2+} concentration slightly increases. This means that it is sufficient to simulate a single action potential in order to determine its influence on the $[Ca^{2+}]_i$. By reducing the problem, it would be more technically feasible to implement spatial dependencies, molecular binding and more complex models of pump/exchanger activity. This in turn would make the model much more accurate.

6.2 Intracellular mechanisms

An essential part of describing the Ca^{2+} response is the intracellular mechanisms. In essence, the LR model behaved reasonably well with high IP3. The Ca^{2+} dynamics between ER and cytosol allowed the $[Ca^{2+}]_i$ to increase.

It was also shown that the ER Ca^{2+} ATPase pump showed unphysiological behavior with stimulus input not explored in the original Li *et al.* article [10]. It was observed that the model showed drastic Ca^{2+} accumulation in the ER, with a constant input through the plasma membrane and IP3 at basal level. Figure 21 illustrates this. It has been experimentally shown that the Ca^{2+} ATPase pumps are more active when the pool it pumps into has a lower concentration [4]. The LR model of pumps and exchangers however does not take into account the Ca^{2+} concentration of the pool it pumps into. Conclusively our simulations illustrates the weakness of the enzymatic mathematical model described by equation 17 regarding the Ca^{2+} ATPase pump on the ER membrane. However it is not known if other models of the IP3 activated Ca^{2+} channels could have solved this problem.

It should also be emphasized that the LR model of IP3 activated Ca^{2+} channels on the ER membrane may describe something which is not physically equivalent of medaka IP3 channels. Even if IP3 channels in gonadotropes and mammals possess biophysiological similarities, these could have been overshadowed by the set of assumptions made when the LR model were originally developed. The kinetics of the intracellular mechanisms in vivo is complicated, and developing effective simplifications that transition well into other systems seems difficult.

In future work we suggest relying on work such as Young and Kaizer 92 [5], which is tied to fundamental assumptions on how IP3 activated Ca^{2+} channels on the ER membrane work. The key emphasis should lie on developing $IP3$ activated Ca^{2+} channels on the ER membrane, and add suitable pump and exchanger activity on the ER membrane and plasma membrane.

6.3 Biological complexity

Lastly, it should be emphasized that the Ca^{2+} behaviour shown to persist in medaka is very complex, and that the simple model proposed here did not try to account for certain features of it. For example, it has been shown that the first part of biphasic response in reality is partly due to L-type channels, a phenomenon we have ignored [18]. Furthermore, medaka cells even respond with

what looks like a release from ER, when the ER Ca^{2+} stores were supposedly empty[18]. In addition, also other ion channels such as SK(small current) and BK (big current) are believed to play a major role in the voltage/Ca^{2+} dynamics of medaka [18]. However, we believe that this model serves as a prototype for future work. After all, we showed that the Li *et al.* model of intracellular Ca^{2+}, in conjunction with Hodgkin Huxley type model of VACC, were able to reproduce the biphasic response observed in medaka.

7 Appendix

7.1 How to solve the equations

In this section we will summarize all the equations needed in order to reproduce our results. The equations which has to be solved together are:

$$C_m \frac{dV}{dt} = -10^{-3} P_{Ca} m_{Ca}^2 G(V_m, [Ca^{2+}]_i \cdot 10^{-3}, [Ca^{2+}]_e - \bar{g}_L(V - E_{Leak}) - \bar{g}_{Na} m^3 h_{Na}(V - E_{Na}) - \bar{g}_K n^4 (V - E_K) - i_{input}) \cdot 10^3 \quad (54)$$

$$dm/dt = (m_\infty - m)/\tau_m \cdot 10^3 \quad (55)$$

$$dh_{Na}/dt = (h_{Na\infty} - h_{Na})/\tau_{h_{Na}} \cdot 10^3 \quad (56)$$

$$dn/dt = (n_\infty - n)/\tau_n \cdot 10^3 \quad (57)$$

$$dm_{Ca}/dt = (m_{Ca\infty} - m_{Ca}/\tau_{m_{Ca}}) \cdot 10^3 \quad (58)$$

Where we have squared with 10^3 to change t from units of ms to s. $G(V_m, [Ca^{2+}]_i, [Ca^{2+}]_e)$ is given by equation 45 in section 4.5.2. m_∞ is given by equation 22, τ_m is given by equation 23, $h_{Na\infty}$ is given by equation 25 , $\tau_{h_{Na}}$ is given by equation 26, n_∞ is given by equation 29 and τ_n is given by equation 28 all of which are described in section 4.2.1. $m_{Ca\infty}$ and $\tau_{m_{Ca}}$ is given by is given by equation 32 and 31 respectively in section 4.2.2. For the Ca^{2+} dynamics we use the rewritten equations from section 4.5.3:

$$\frac{d[Ca^{2+}]_i}{dt} = ((p_{leak} + O)([Ca^{2+}]_{er} - [Ca^{2+}]_i) - j_{er,p} - (j_{m,p} + j_{m,Na/Ca})\epsilon/\lambda + J_{m,in}/(V_i f_i) \quad (59)$$

$$dh/dt = (h_\infty - h)/\tau_h \quad (60)$$

$$\frac{d[Ca^{2+}]_T}{dt} = -(j_{m,p} + j_{m,Na/Ca})\epsilon/\lambda + J_{m,in}/(V_i f_i) \quad (61)$$

Where $[Ca^{2+}]_{er} = ([Ca^{2+}]_T - [Ca^{2+}]_i)/\sigma_{er}$. And $O = a_\infty b_\infty d_\infty h$. a_∞ is given by equation 35, b_∞ is given by 36, d_∞ is given by 37 and τ_h is given by equation 40 all of which are listed in section 4.3. The pumps and exchangers activities are given by equation [10]:

$$j_x = v_x [Ca^{2+}]_i^{n_x} / ([Ca^{2+}]_i^{n_x} + K_i^{n_x}) \tag{62}$$

Where relevant parameters are listed in table 2. The current into the cell is $J_{m,in} = \frac{A}{2F} i_{Ca}$ where $i_{Ca} = 10^{-3} \bar{g}_L m_{Ca}^2 G(V_m, [Ca^{2+}]_i, [Ca^{2+}]_e)$.

Table 1: Voltage parameters

Parameter	Description	Model value	reference/source
E_K	K^+ equilibrium potential	$-90\,\mathrm{mV}$	[6]
E_{Na}	Na^+ equilibrium potential	$50\,\mathrm{mV}$	[6]
E_L	Leak equilibrium potential	$-65.4\,\mathrm{mV}$	[16] p. 61
$\bar{g}_{Na}$	Na^+ conductance	$4\,\mathrm{mS\,cm^{-2}}$	-
$\bar{g}_K$	K^+ conductance	$0.7\,\mathrm{mS\,cm^{-2}}$	-
$\bar{g}_L$	Leak conductance	$0.3\,\mathrm{mS\,cm^{-2}}$	-
C_m	Membrane capacitance	$1.0\,\mu\mathrm{F\,cm^{-2}}$	[16] p. 61
P_{Ca}	L-channel permeability	$0.2\,\mathrm{dam\,s^{-1}}$	-
$[Ca^{2+}]_e$	extracellular Ca^{2+} concentration	$1.4\,\mu\mathrm{M}$	[19]
$i_{input,2}$	Input current generating 2 Hz AP frequency	$3.5904\,\mu\mathrm{A\,cm^{-2}}$	-
$i_{input,1}$	input current which gives 1 Hz AP frequency	$3.589\,85\,\mu\mathrm{A\,cm^{-2}}$	-
T	Temperature for Na^+ /K^+ ion channel kinetics	$34\,^\circ\mathrm{C}$	-
T_{Ca}	Temperature used in L-type current equation	$300\,\mathrm{K}$	-
R	the gas constant	$8.314\,459\,8\,\mathrm{J\,mol^{-1}\,K^{-1}}$	[21]
F	Faraday's constant	$96\,485.33\,\mathrm{C\,mol^{-1}}$	[20]

Table 2: LR parameters

Parameter	Description	Model value	reference/source
σ_{er}	$V_{er}f_i/V_if_{er}$	0.7	[10]
λ	$V_i/P_{ip3r}f_i$	0.3	[10]
f_i	Fraction of free Ca^{2+} in cytosol	0.01	[10]
f_{er}	Fraction of free Ca^{2+} in ER	0.0025	[10]
C_i^0	Initial Ca^{2+} concentration	$0.2\,\mu\mathrm{M}$	[10]
h^0	IP3 activated opening variable	0.8	[10]
$[Ca^{2+}]_T^0$	$[Ca^{2+}]_i^0 + \sigma_{er}[Ca^{2+}]_{er}^0$	$3.5\,\mu\mathrm{M}$	[10]
$p_{er,l}$	ER leak permeability	0.0005 dimensionless	[10]
ϵ	A_{pl}/A_{er}	0.01 dimensionless	[10]
$v_{er,p}$	pump rate into ER	$0.245\,\mu\mathrm{M}$	see eq. 62, [10]
$v_{m,p}$	passive pump rate plasma membrane	$0.3\,\mu\mathrm{M}$	see eq. 62, [10]
$v_{m,Na/Ca}$	Na/Ca^{2+} exchanger rate	$7.0\,\mu\mathrm{M}$	see eq. 62, [10]
$K_{er,p}$	pump rate into ER, see equation	$0.15\,\mu\mathrm{M}$	see eq. 62, [10]
$K_{m,p}$	passive pump rate plasma membrane	$0.3\,\mu\mathrm{M}$	see eq. 62, [10]
$K_{m,Na/Ca}$	Na/Ca^{2+} exchanger rate	$0.9\,\mu\mathrm{M}$	see eq. 62, [10]
$n_{er,p}$	Hill coefficient	2 unitless	see eq. 62, [10]
$n_{m,p}$	Hill coefficient	2 unitless	see eq. 62, [10]
$n_{m,NaCa}$	Na/Ca^{2+} exchanger Hill Coefficient	4 unitless	see eq. 62, [10]
d_{cell}	Cell diameter	$10\,\mu\mathrm{m}$	[18]
V_i	Volume cytosol	(in liters)	$\frac{4\pi}{3}(d_{cell}/2)^3$
A	Surface area cell	(in cm^2)	$4\pi(d_{cell}/2)^2$
$j_{m,in}$	Constant Ca^{2+} into cell	$0.175\,\mu\mathrm{M}$	see eq. 63 [10]

7.2 Conversion of units

In this subsection we will present how Ca^{2+} fluxes as calculated from 62 is calculated back to our physical representative quantities as expressed in section 4.3. For $J_{m,NaCa}$ and $J_{m,p}$ we use equation 50 and equation 48.

$$J_{m,NaCa} = j_{m,NaCa}\epsilon P_{ip3r}$$

and using equation 48:

$$J_{m,NaCa} = j_{m,NaCa}\epsilon \frac{V_i}{\lambda f_i}$$

and same with $J_{m,p}$:

$$J_{m,p} = j_{m,p}\epsilon \frac{V_i}{\lambda f_i}$$

On the other hand $J_{er,p}$ we get with equation 51:

$$J_{er,p} = j_{er,p}P_{ip3r}$$

which is

$$J_{er,p} = j_{er,p}\frac{V_i}{\lambda f_i}$$

The pump rates as mentioned in 4.3 is:

$$V_{m,NaCa} = \epsilon P_{ip3r} v_{m,NaCa}$$

$$V_{m,p} = \epsilon P_{ip3r} v_{m,p}$$

$$V_{er,p} = P_{ip3r} v_{er,p}$$

Sometimes we use the $J_{m,in}$ flux denoted with lower case: $j_{m,in}$. This is the original input current in the Li *et al.* model [10]. This flux has same units as $j_{m,NaCa}$ and $j_{m,p}$:

$$j_{m,in} = J_{m,in}\frac{\lambda f_i}{V_i \epsilon} \tag{63}$$

References

[1] C. Acuna-Goycolea, S. D. Brenowitz, and W. G. Regehr. Active dendritic conductances dynamically regulate gaba release from thalamic interneurons. *Neuron*, 57(3):420–431, 2008.

[2] W. A. Catterall, K. Leal, and E. Nanou. Calcium channels and short-term synaptic plasticity. *Journal of Biological Chemistry*, 288(15):10742–10749, 2013.

[3] D. E. Clapham. Calcium signaling. *Cell*, 131(6):1047–1058, 2007.

[4] E. De Schutter and P. Smolen. Calcium dynamics in large neuronal models. *Methods in neuronal modeling: From ions to networks*, 2, 1998.

[5] G. W. De Young and J. Keizer. A single-pool inositol 1, 4, 5-trisphosphate-receptor-based model for agonist-stimulated oscillations in ca2+ concentration. *Proceedings of the National Academy of Sciences*, 89(20):9895–9899, 1992.

[6] G. Halnes, S. Augustinaite, P. Heggelund, G. T. Einevoll, and M. Migliore. A multi-compartment model for interneurons in the dorsal lateral geniculate nucleus. *PLoS Comput. Biol.*, 7(9):e1002160, Sep 2011.

[7] B. Hille et al. *Ion channels of excitable membranes*, volume 507. Sinauer Sunderland, MA, 2001.

[8] C. M. Johnson, C. S. Hill, S. Chawla, R. Treisman, and H. Bading. Calcium controls gene expression via three distinct pathways that can function independently of the ras/mitogen-activated protein kinases (erks) signaling cascade. *The Journal of neuroscience*, 17(16):6189–6202, 1997.

[9] Y.-X. Li and J. Rinzel. Equations for insp 3 receptor-mediated [ca 2+] i oscillations derived from a detailed kinetic model: a hodgkin-huxley like formalism. *Journal of theoretical Biology*, 166(4):461–473, 1994.

[10] Y. X. Li, J. Rinzel, J. Keizer, and S. S. Stojilkovi? Calcium oscillations in pituitary gonadotrophs: comparison of experiment and theory. *Proc. Natl. Acad. Sci. U.S.A.*, 91(1):58–62, Jan 1994.

[11] Y.-X. Li, J. Rinzel, L. Vergara, and S. Stojilković. Spontaneous electrical and calcium oscillations in unstimulated pituitary gonadotrophs. *Biophysical journal*, 69(3):785, 1995.

[12] P. Nelson and S. Doniach. Biological physics: Energy, information life. *Physics Today*, 57(11):63–64, 2004.

[13] F. Rieke. Hodgkin huxley equivalent circuit. `http://rieke-server.physiol.washington.edu/People/Fred/Classes/532/HH1_11.pdf`, 2011.

[14] G. D. Smith. Analytical steady-state solution to the rapid buffering approximation near an open ca2+ channel. *Biophysical journal*, 71(6):3064, 1996.

[15] J. Sneyd and J.-F. Dufour. A dynamic model of the type-2 inositol trisphosphate receptor. *Proceedings of the National Academy of Sciences*, 99(4):2398–2403, 2002.

[16] D. Sterratt, B. Graham, A. Gillies, and D. Willshaw. *Principles of computational modelling in neuroscience*. Cambridge University Press, Cambridge, New York, 2011. Machine generated contents note: Preface; 1. Introduction; 2. The basis of electrical activity in the neuron; 3. The Hodgkin Huxley model of the action potential; 4. Compartmental models; 5. Models of active ion channels; 6. Intracellular mechanisms; 7. The synapse; 8. Simplified models of neurons; 9. Networks; 10. The development of the nervous system; Appendix A. Resources; Appendix B. Mathematical methods; References.

[17] R. A. Strandabø, H. K. Grønlien, E. Ager-Wick, R. Nourizadeh-Lillabadi, J. P. Hildahl, F.-A. Weltzien, and T. M. Haug. Identified lhb-expressing cells from medaka (oryzias latipes) show similar ca 2+-response to all endogenous gnrh forms, and reveal expression of a novel fourth gnrh receptor. *General and comparative endocrinology*, 229:19–31, 2016.

[18] R. A. Strandabø, K. Hodne, E. Ager-Wick, O. Sand, F.-A. Weltzien, and T. M. Haug. Signal transduction involved in gnrh2-stimulation of identified lh-producing gonadotropes from lhb-gfp transgenic medaka (oryzias latipes). *Molecular and cellular endocrinology*, 372(1):128–139, 2013.

[19] unknown. Extracellular calcium ion concentration. `http://www.alzet.com/products/guide_to_use/cfs_preparation.html`, 2016.

[20] unknown. Faraday's constant. `http://physics.nist.gov/cgi-bin/cuu/Value?f`, 2016.

[21] unknown. The gas constant. `http://physics.nist.gov/cgi-bin/cuu/Value?r`, 2016.

[22] unknown. odepack, fortran77 library. `https://people.sc.fsu.edu/~jburkardt/f77_src/odepack/odepack.html`, 2016.

[23] unknown. Python memory. `https://docs.python.org/2/c-api/memory.html`, 2016.

[24] unknown. scipy.integrate.odeint. `http://docs.scipy.org/doc/scipy-0.16.0/reference/generated/scipy.integrate.odeint.html`, 2016.

[25] D. Young and . Keizer. (de young and keizer, 1992). *(De Young and Keizer, 1992)*, 372(1):128–139, 2013.

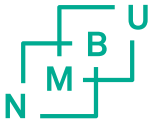

Norges miljø- og biovitenskapelig universitet
Noregs miljø- og biovitskapelege universitet
Norwegian University of Life Sciences

Postboks 5003
NO-1432 Ås
Norway